An OPC UA Client/Gateway-based Architecture for SCADA Systems with Automatic Mental Fatigue Detection Application

by

Ahmad Abdelsattar

B.Sc. (Hons.), Arab Academy for Science and Technology, 2020

Thesis Submitted in Partial Fulfillment of the
Requirements for the Degree of
Master of Applied Science

in the
School of Mechatronic Systems Engineering
Faculty of Applied Sciences

SIMON FRASER UNIVERSITY
Spring 2023

Declaration of Committee

Name:	**Ahmad Abdelsattar**
Degree:	**Master of Applied Science**
Title:	**An OPC UA Client/Gateway-based Architecture for SCADA Systems with Automatic Mental Fatigue Detection Application**
Committee:	**Chair:** **Ramtin Rakhsha** Lecturer, Mechatronic Systems Engineering
	Edward J. Park Co-Supervisor Professor, Mechatronic Systems Engineering
	Amr Marzouk Co-Supervisor Senior Lecturer, Mechatronic Systems Engineering
	Mehrdad Moallem Committee Member Professor, Mechatronic Systems Engineering
	Farshid Najafi Examiner Assistant Professor, Mechatronic Systems Engineering

Ethics Statement

The author, whose name appears on the title page of this work, has obtained, for the research described in this work, either:

a. human research ethics approval from the Simon Fraser University Office of Research Ethics

or

b. advance approval of the animal care protocol from the University Animal Care Committee of Simon Fraser University

or has conducted the research

c. as a co-investigator, collaborator, or research assistant in a research project approved in advance.

A copy of the approval letter has been filed with the Theses Office of the University Library at the time of submission of this thesis or project.

The original application for approval and letter of approval are filed with the relevant offices. Inquiries may be directed to those authorities.

Simon Fraser University Library
Burnaby, British Columbia, Canada

Update Spring 2016

Abstract

With the emergence of Industry 4.0 concepts, including digital twins, traditional Supervisory Control and Data Acquisition (SCADA) systems impose significant restrictions on the interoperable communication between machines that use various Industrial Internet-of-Things (IIoT) devices. Also, recent Internet-of-Things (IoT) advancements led to the development of the analogous Operator 4.0 concept, which focuses on augmenting workers with technology (e.g., using wearable IoT devices that can monitor workers' health conditions) and constructing "human" digital twins. This thesis presents a new smart factory concept that consists of integrated and interoperable manufacturing machine and human (i.e., worker) digital twin units. First, a new data exchange architecture based on Open Platform Communication protocol Unified Architecture (OPC UA) was developed and tested to create a digital twin of an IIoT device and monitor real-time sensor data. Second, the architecture further incorporated a newly developed and tested mental fatigue detection technique based on wearable photoplethysmography (PPG) sensor readings to create a human's digital twin unit that monitors a worker's mental fatigue to mitigate potential safety risks. Such an integration facilitates real-time monitoring of both machines' processing parameters and factory workers' physiological parameters simultaneously. Experimental results demonstrate the proof-of-concept of the new data exchange architecture in creating interoperable and non-restricted machine and human digital twin units for smart factories.

Keywords: Industry 4.0; Smart Factory; Digital Twin; Internet of Things; Mental Fatigue; Photoplethysmography; Heart Rate Variability; Machine Learning

Dedication

To my family Talaat, Manal, Menna and Afreen

Whose love, encouragement and support make me able to achieve such success and honor

Acknowledgements

I would like to express my gratitude towards my senior supervisor, Dr. Edward Park, for giving me the opportunity to join his research team and obtain my master's degree. From the moment I joined his team, he has been patiently guiding and teaching me through my degree. I have learned valuable skills for conducting research and writing academic papers by following his priceless recommendations and feedback on my research work.

I would like to thank and am very grateful to Dr. Amr Marzouk for his guidance. Also, for reviewing my academic materials and providing me with technical solutions for hands-on problems. I would like to thank Dr. Mehrdad Moallem for taking his time to provide me with invaluable feedback on my research. I would also like to thank Dr. Farshid Najafi for the time he spent examining my work and providing constructive feedback.

I would like to thank all members of WearTech and Biomechatronics Labs at the School of Mechatronic Systems Engineering for their support and help they provided throughout my research. A special thanks to Dominic Jaworski for guiding me and providing me with helpful materials. I would like to thank Taha Al-Khudairi, Osama Al-Humaimidi and Zainulabdin Khanzada for their technical support. Also, I would like to thank my friends Abdelrahman Al-Domyati and Omar Nemir for their unlimited support throughout my degree.

Lastly, I would like to thank my family, Talaat, Manal, Menna and Afreen for their endless support and guidance throughout the tough days. With your love and encouragement, I was able to go way beyond my limits.

Table of Contents

Declaration of Committee ii
Ethics Statement iii
Abstract iv
Dedication v
Acknowledgements vi
Table of Contents vii
List of Tables ix
List of Figures x
List of Acronyms xi
Glossary xiii

Chapter 1. Introduction 1
1.1. Background 5
1.1.1. SCADA Systems Architecture 5
1.1.2. Fatigue Detection 7
1.2. Objectives 8
1.3. Contributions 8
1.4. Thesis Overview 9

Chapter 2. Client/Gateway-Based Architecture 10
2.1. Literature Review 10
2.2. The Proposed Architecture 14
2.2.1. Client/Gateway Node 14
2.2.2. Server Nodes 15
2.2.3. Cloud Services 16
2.2.4. End-User Nodes 16
2.3. Application Case Study 16
2.3.1. Case Study: FESTO MPS 16
2.3.2. Case Study: Architecture 17
2.3.3. Case Study: Server Nodes 18
2.3.4. Case Study: Gateway and Users Nodes 19
2.4. Results 20
2.4.1. Latency Results 21
2.4.2. Raspberry Pi CPU Usage and Temperature 22
2.4.3. Limitations 23
2.5. Summary 23

Chapter 3. Mental Fatigue Detection 24
3.1. Literature Review 24
3.1.1. EEG 24
3.1.2. ECG 25
3.1.3. PPG 27

3.2. Study Materials and Methods 27
3.2.1. Participants 27
3.2.2. Hardware and Software 28
3.2.3. Experimental Design 30
3.2.4. Data Preprocessing 31
3.3. Results 36
3.3.1. Feature Selection 36
3.3.2. Machine Learning Classifiers 39
3.3.3. Automatic Detection via a Moving Window 41
3.4. Discussion 43
3.4.1. Main Findings 43
3.4.2. Comparison with Relevant Work 48
3.4.3. Limitations and Proposed Solutions 49
3.5. Application Case Study: A Connection with The Proposed Client/Gateway Architecture 49
3.5.1. Integration within Smart Factory 49
3.5.2. Raspberry Pi CPU Utilization and Temperature 51
3.5.3. Potential Real-Life Implementation Scenarios 53
3.6. Summary 53

Chapter 4. Conclusions 55
4.1. Conclusions 55
4.2. Future Work 57

References 58

Appendix A. Ethics Approval 69

Appendix B. Consent Form 70

Appendix C. Significant Features Box Plots 75

Appendix D. ANOVA Scores 78

Appendix E. HRV Features for All Participants 85

List of Tables

Table 2.1. Servers Timestamps 21
Table 3.1. Chalder Fatigue Scale Questionnaire.....31
Table 3.2. Statistically Significant HRV Parameters 37
Table 3.3. Gini Index and ANOVA Scores For Statistically Significant Features.....38
Table 3.4. Comparison of Machine Learning Classifiers' Performance 41
Table 3.5. VitalStream Vs DFRobot Error Comparison 47

List of Figures

Figure 2.1. OPC UA client/gateway-based architecture in a smart factory. 14
Figure 2.2. FESTO MPS Processing Station. 17
Figure 2.3. Case study architecture with Raspberry Pi and Siemens PLC running OPC UA servers. 18
Figure 2.4. Ignition Perspective SCADA screen on a portable device. 20
Figure 2.5. Raspberry Pi CPU usage and temperature while in operation. Spikes in the CPU usage and temperature occur upon establishing a new connection. 22
Figure 3.1. QRS complex for three consecutive heartbeats [48]. 25
Figure 3.2. A) PPG sensor attached to the index finger, which is connected to the Arduino Uno. B) Advanced Trail Making Test session running on a commercial tablet. C) NASA Psychomotor Vigilance Test session with a reaction timer (in ms) shown in the bottom box. 29
Figure 3.3. Three seconds of PPG readings with peaks detected. 29
Figure 3.4. Experiment timeline starting with self-report questionnaire at rest state and ending with a second round of the survey at fatigue state. 30
Figure 3.5. Flowchart of the proposed feature selection process from the collection of participants' data to feeding extracted HRV features into the machine learning models. 38
Figure 3.6. NNI durations for a participant at rest and fatigue states for the first 40 intervals which approximately correspond to the first 30 seconds. 39
Figure 3.7. Automatic fatigue detection via moving window using LR, ANN, NB, and KNN machine learning models. 43
Figure 3.8. A) NNI_20 count for all participants with the blue bar representing the rest state and the orange bar representing the fatigue state. B) Box plot showing the difference in NNI_20 between males and females at rest state (left side) versus fatigue state (right side) with the orange bar representing the median. 44
Figure 3.9. A) The reaction times of all participants with the blue bar representing the rest state and the orange bar representing the fatigue state. B) Box plot showing the difference in reaction time between males and females at rest state (left side) versus fatigue (right side) with the orange bar representing the median. 46
Figure 3.10. VitalStream device in the calibration mode. 48
Figure 3.11. Human digital twin unit to monitor mental fatigue status. 50
Figure 3.12. The alarm screen on Ignition Perspective. 51
Figure 3.13 Raspberry Pi CPU Temperature and Utilization with ANN Classifier. The CPU utilization is presented by the blue color and the temperature is represented by the orange color. 52

List of Acronyms

ANN	Artificial Neural Network classifier
ANOVA	Analysis of variance
ATMT	Advanced Trail Making Test
CPS	Cyber-Physical System
CPU	Central processing unit
DT	Decision Tree Classifier
ECG	Electrocardiography
EEG	Electroencephalogram
FDA	Food and Drug Administration
HCPS	Human Cyber-Physical System
HF	High frequency
HFnu	Normalized high frequency
HMI	Human Machine Interface
HRV	Heart rate variability
Industry 4.0	Fourth industrial revolution
LF	Low frequency
LF/HF	Low to high frequency
LFnu	Normalized low frequency
LR	Logistic Regressor classifier
Mean_NNI	The mean of normal-to-normal-intervals.
Median_NNI	Median absolute values of the successive differences between the normal-to-normal-intervals.
NNI	Normal-to-normal intervals
NNI_20	Number of interval differences of successive NN-intervals greater than 20 ms
NNI_50	Number of interval differences of successive NN-intervals greater than 50 ms
OPC UA	Open Platform Communication Unified Architecture
PLC	Programmable Logic Controller
PPG	Photoplethysmography

PSNS	Parasympathetic nervous system
PVT	Psychomotor Vigilance Test
RF	Random Forest classifier
RMSSD	Root mean square of successive differences between normal heartbeats
SCADA	Supervisory Control and Data Acquisition
SDNN	Standard deviation of normal-to-normal
SDSD	Standard deviation of successive normal-to-normal interval differences
SGD	Stochastic Gradient Descent classifier
SNS	Sympathetic nervous system
Std_HR	Standard deviation of heart rate
SVM	Support Vector Machine classifier
UART	Universal Asynchronous Receiver Transmitter
XGBoost	Extreme Gradient Boost classifier

Glossary

Cyber-Physical System	Physical systems that require monitoring, coordination, control, and data integration managed and connected by a computing unit
Digital Twin	A digital replica of a physical entity
Heart Rate Variability	The variance in duration between successive heartbeats
Human Cyber-Physical Systems	Systems designed to fit and improve human or worker's abilities (physical and cognitive) to perform tasks and interact with machines both cyber and physical worlds
Ignition®	A SCADA software includes OPC UA, HMI design and programming, alarms, reports and tag historian modules
Latency	The time between sending the data and acknowledgment of receiving
Mental Fatigue	A state when a person's abilities to perform mental tasks significantly drop
Normal-to-normal interval	The duration between two consecutive heart beats
Parasympathetic Nervous System	Part of nervous system that regulates the heartbeats at rest
QRS complex	Heart rate deflection presented in ECG recordings
Sympathetic Nervous System	Part of nervous system that regulates the heartbeats at fatigue

Chapter 1.

Introduction

Cyber-physical system(s) (CPS) relate to integrated hardware and software components that interact with physical processes in real-time [1]. Physical systems that require monitoring, coordination, control, and data integration, managed and connected by a computing unit, can be referred to as CPS [2]. Moreover, for a system to be classified as a true CPS, every possible physical component must have an embedded controlling component for monitoring and control purposes, if applicable, alongside a central control unit [1]. Wang et al. [3] discussed early applications of CPS such as asset identification and tracking by equipping physical objects and components with identification devices such as Radio Frequency Identification (RFID) tags. The concept of CPS has significantly evolved to connect subsystems that include sensors, actuators, and process controllers. This communication between system components within a CPS can facilitate real-time system monitoring, fault detection, and troubleshooting. Currently, smart manufacturing is considered one of the main applications of CPS technologies [1].

Theoretically, Internet of Things (IoT) technologies allow any object to communicate with other objects, ”things,” regardless of their location or distance [4]. Researchers have investigated methods to incorporate IoT technologies to improve production and construct CPS. Dafflon et al. [5] discussed the integration of IoT technologies within production plants as one of the applications of Industry 4.0 and Industrial Internet of Things (IIoT). Industry 4.0, referred to as the fourth industrial revolution, involves digital transformation of factories. A CPS in the context of Industry 4.0 consists of three elements: (i) physical component, (ii) cyber component, and (iii) human component [5].

The physical components of CPS, such as robots, material shaping and handling machines controlled by industrial controllers that communicate using Machine-to-Machine (M2M) protocols, are considered a vital component of CPS [6]. This interconnectivity allows machine coordination and decouples decision making from the central control unit, while complying with the production objectives [7]. Achieving a completely decentralized autonomous factory decreases production costs and allows for

more customized manufacturing orders [8]. It can significantly decrease troubleshooting and maintenance time.

The cyber component of CPS includes virtualization. It can be defined as forming a virtual environment for monitoring, controlling, and simulating physical parts of a CPS [7]. A virtual replica that reflects the status, performs simulations, and analyzes the behaviour of its physical counterpart is referred to as a digital twin [9], [10]. Zawadzki and Żywicki [11] discussed virtual commissioning, which is the simulation of a digital twin of a production line or individual machines to be configured, tested, and analyzed virtually prior to physical deployment. Additionally, a digital twin can be used to facilitate training of machine operators through complex operations, troubleshooting, and maintenance. Faults, internal components, and servicing can be interactively displayed via augmented reality (AR) or virtual reality (VR). The advancements of human-machine interaction in both the cyber and physical world led to the development of Human Cyber-Physical System(s) (HCPS).

HCPS can be defined as systems designed to fit and improve a human or worker's abilities (physical and cognitive) to perform tasks and interact with machines [12]. As workers interact with physical machines within a CPS, human-physical and human-cyber interactions are the observed types of interactions [13]. The concept of Operator 4.0 emerged following the main objective of HCPS, which is enhancing operators' abilities using HCPS to perform tasks.

In the context of Operator 4.0, human-physical interaction within an HCPS, Ansari et al. [14] developed a framework that allows a robot arm to mimic and learn from the movement of its operator without pre-programming. Bandala et al. [15] developed a teleoperation technique that allows operators to remote-control robots using joysticks and remote vision systems. Deng et al. [16] developed a facial expression detection algorithm to allow robots to understand its operators' emotions and health state. As a result, emergency protocols can be initiated by announcing alarms to ensure the safety of operators in high-risk situations.

On the Operator 4.0 human-cyber side and, as previously mentioned, AR and VR, are emerging technologies that play a vital role in providing operators with an

immersive experience to assist in performing complex tasks and mitigate physical risks [17]. In this context, Longo et al. [18] developed SOPHOS-MS, an application that facilitates operators' CNC training in a virtual environment. The training involved pneumatic and hydraulic system maintenance, an operator panel, tool changing, as well as lubrication and coolant systems. A pair of Samsung Gear VR glasses was used for visualization alongside Myo Armbands for gesture recognition. In addition, a monocular glass with motion capture armbands was utilized in the AR version of SOPHOS-MS. Salah et al. [19] conducted an experiment using two groups trained on an Industry 4.0-reconfigurable manufacturing system. The first group was trained using VR while the second received traditional classroom training. The VR group results showed a significant improvement in terms of completion time and fewer errors.

Another aspect of interest of Operator 4.0 human-cyber interaction is the machine operator's health and safety. Advancements in wearable IoT devices enabled health monitoring of machine operators in real-time. Vital signs and activities using wearable devices could be measured in addition to position tracking to report incident locations in remote or low visibility environments [13], [20]. In this context, Sun et al. [17] developed a framework that consisted of multiple layers for modeling and monitoring the health conditions of operators, a crane operator in their case. In the sensing layer, sensors were designed to monitor the operator's work environment (e.g., temperature, humidity, and noise). Also, an off-the-shelf smart band from HBand was utilized to monitor the operator's heart rate (HR), blood pressure, and steps. Ultra-wide band (UWB) anchors and tags were installed to monitor the crane's exact location and movements within a work site. On the integration side, an Android application was developed from scratch to integrate and interpret dissimilar data structures generated by the sensors. The experimental setup only showed efficacy in monitoring different sensors and generating reports from stored data, not in using the data.

In HCPSs in the context of Industry 4.0, a smart factory consists of connected and pervasive systems that provide inputs to the digital twin of the factory floor, which can monitor both manufacturing processes and factory floor safety. This thesis explores some of the key HCPS concepts within Industry 4.0 by proposing a new data exchange architecture and integrating it with fatigue detection to improve factory worker safety as part of the Operator 4.0 concept in a smart factory.

In our smart factory concept, all machines as well as workers are considered physical entities in compliance with the HCPS concept. Every physical entity can be represented by a digital twin within the smart factory. For example, a machine digital twin simulates, represents, controls, and stores a machine's parameters such as running status and speed in real-time [21]. Hence, our smart factory concept consists of two elements: (i) machines' digital twin units and (ii) workers' digital twin units. Both digital twin elements communicate without any restrictions (i.e., a machine can be connected to its operator through a communication channel). Traditionally, on the machine side, Supervisory Control and Data Acquisition (SCADA) systems were only capable of transferring data between local and vendor-specific equipment, and certain compatible hardware and software. Also, SCADA systems restricted the integration of wearable IoT devices that are controlled by embedded controllers. Thus, traditional SCADA systems lack interoperable machine-to-machine (M2M) communication, which limits the full capabilities of digital twins in Industry 4.0, where all digital twin units are connected with each other regardless of their manufacturer [10]. With the recent advancements of IIoT concepts that focus on interoperable M2M communication and connection to the Internet, effective digital twin units can be constructed [6].

As mentioned earlier, the utilization of IoT devices in the area of monitoring the health conditions of workers within an HCPS as a part of the Operator 4.0 concept. One of the key elements of the Operator 4.0 concept is extracting and uploading various physiological and pathological signals to the Internet or a cloud service in real-time. For example, and similar to Sun et al. [17], Shaikh and Chitre [22] developed a health monitoring system using a Raspberry Pi, which is their IoT device of choice that reports to the Internet, connected to various physiological sensors for temperature, electrocardiography (ECG), HR, and blood pressure. Similarly, Kumar and Rajasekaran [23] connected similar physiological sensors (for temperature, respiration rate, and HR) with a Raspberry Pi that uploads the patient's data to a website, which can be accessed by the healthcare provider. In these cases, a digital twin unit for an individual that monitors, stores, and provides data-driven health-related suggestions is formed. Although the machine and human digital twin concepts and technologies provide analogous data structures for different objects (i.e., machines' digital twins in Industry 4.0 and humans' digital twins in Operator 4.0), an integration between these two concepts has not been explored previously. Such an integration facilitates real time

monitoring of both machines' processing parameters and factory workers' physiological parameters simultaneously. Therefore, when an alarm is triggered to a unit within the smart factory based on monitored parameters of either machines or humans, associated units can be notified so that an action can be taken. For example, a worker's digital twin unit that predicts and reports potential health issues to other digital twin units as well as the supervisory system can mitigate potential safety risks [24], [25].

In this thesis, our main health condition of interest as part of the Operator 4.0 and Industry 4.0 setting is mental fatigue, considering its adverse effects on workers' productivity and safety that are further discussed in Chapter 1.1.2. Recalling our overall smart factory concept introduced above, a wearable IoT device worn by a worker forms a worker's digital twin unit that reports their current fatigue state to the main shop floor digital twin. Consequently, the shop floor digital twin may force the corresponding physical machine to stop if there is an increased risk of injury due to the worker's fatigued condition. Herein, the integration of both digital twin unit types, machine and human digital twins, was enabled using the new data exchange architecture mentioned earlier. Furthermore, a novel fatigue detection method was developed, tested, and incorporated into the architecture as a proof-of-concept demonstration.

Chapter 1.1.1 provides a background about the Industry 4.0 concept, evolution, and IoT enabled wearable devices. Chapter 1.1.2 provides a background about fatigue as the health condition of interest. Chapter 1.2 lists the main objectives of this thesis. Chapter 1.3 summarizes the contributions of this work. Finally, Chapter 1.4 lists the thesis overview and structure.

1.1. Background

Our work presented in Chapter 1.1.1, Chapter 2, and part of Chapter 4 was presented and published in IEEE Xplore and can be found in [26].

1.1.1. SCADA Systems Architecture

SCADA was developed to monitor and control plant states from a centralized location in real time. This enabled the automation of industrial processes, as well as the development of simplified digital representations of those processes for visualizing

system states. Židek et al. [27] suggested that all manufacturing systems, including their physical components and products, can be digitalized in theory. In this context, as a digital bridge between the plant floor and the higher-level systems, new SCADA systems have been researched over the years in terms of different bridging connectivity architectures [28].

Although SCADA systems have been used intensively in the manufacturing sector, SCADA concepts and implementations still have major drawbacks. For example, traditional SCADA systems lack interoperability that allows different equipment provided by various vendors to communicate with each other within the shop floor. Therefore, conventional SCADA systems are not capable of performing complex tasks beyond simple process monitoring and control. In addition, larger SCADA networks that include remote devices are more vulnerable to cyber-attacks and require more cybersecurity attention [28]. Another major drawback is the significant capital that needs to be invested to purchase and setup the SCADA equipment [29].

In the context of SCADA systems equipment communication, Ethernet technology lacks real-time communication which led to the development of industrial Ethernet. Moreover, industrial Ethernet was also proven incompatible with the traditional Ethernet standard in numerous cases [30]. Communication standards such as ProfiNET, POWERLINK, and EtherCAT are a few standards based on the industrial Ethernet concept. ProfiNET has layers analogous to the ISO/OSI model, but also lacks the interoperability between devices supporting different industrial Ethernet protocols. This major drawback has driven the development of the Open Platform Communication (OPC).

The OPC concept was developed by Microsoft in early 90’s. In 1995, Fisher-Rosemount, Intellution, Opto 22, and Rockwell Software agreed to start developing a standard for data transformation and access based on the OPC, and a year after OPC Data Acquisition (DA) version 1.0 was released. A continued development of the new protocol followed after that, including the conversion of some of the specifications into web-based services and the emergence of the Internet in the late 90’s. In 2006, Open Platform Communication Unified Architecture (OPC UA) was introduced and became available for all manufacturers. In addition, certification programs and test labs were

introduced along with the release. OPC UA now supports connectivity for many different platforms including robotics and machine learning.

To begin with, OPC UA does not necessarily need hardwired Ethernet infrastructure contrarily to its industrial Ethernet counterparts. Also, OPC UA is based on a Server-Client, Publisher/Subscriber (Pub/Sub) model. This allows for more variability in terms of communication between field devices by implementing various network architectures as explained in [31]. Also, OPC UA offers the flexibility of being incorporated into existing software packages written in a variety of programming languages such as C/C++, .NET, Java, and Python without the need for external hardware components. In this work, the utilisation of OPC UA communication protocol is proposed for the development of our digital twin concept/architecture for smart factories.

1.1.2. Fatigue Detection

Fatigue can be described as the periods during which workers' performance and productivity decline due to extended shifts [32], [33]. Cerebrovascular/cardiovascular diseases (CVDs) as well as mental fatigue resulting from extreme work conditions are shown to be highly associated with workers' health complications [34]–[36]. Mental (or cognitive) fatigue is a state that describes the person's feeling of tiredness, lack of energy, and disrupted ability to perform mental tasks [37], [38]. According to Sarkar and Parnin's survey [39] on 311 software developers, office workers such as programmers who experience mental fatigue have lower productivity and a higher risk of code malfunctions, which can lead to dangerous conditions (e.g., autopilot or navigation system errors). Over the long term, mental fatigue was shown to contribute to aggravation of symptoms in certain illnesses or, in extreme cases, cause death. The correlation between work-induced stress, mental fatigue, and diseases including CVDs, diabetes, and prostate cancer was presented in [40]–[43].

Researchers have developed different methods to quantify the severity of mental fatigue. These methods include the usage of different physiological sensing modalities such as electroencephalogram (EEG) [44], ECG [45], HR, and blood oxygen saturation level (SpO2) [46]. In this work, a new mental fatigue detection method is proposed based on heart rate variability (HRV) features solely extracted from photoplethysmography (PPG) data.

1.2. Objectives

The first primary objective of this thesis was to develop a generic smart factory architecture that utilizes OPC UA as the main communication protocol. As mentioned in the literature, digital twins include many aspects and can be addressed using various techniques and platforms. However, this thesis aims to integrate embedded systems devices in the generic architecture and incorporate them using the OPC UA protocol. Combining embedded device data and traditional industrial controllers enhances smart factory features and capabilities. For example, the implementation of embedded sensors that can be found in wearable devices enables a continuous monitoring of workers' vitals. Hence, proper actions can be taken in situations of a medical emergency or increased safety risks.

The second primary objective of this thesis was to show the extent to which mental fatigue can be detected using PPG sensors, as the target application of the proposed generic OPC UA-based Industry 4.0 framework for incorporating embedded wearable devices with industrial processes. Wearable sensors such as a PPG monitor connected to an embedded controller can enable fatigue detection by extracting HRV features from PPG readings. Statistically selected HRV features were labelled and then passed to the machine learning models to train them. Trained machine learning models were then used to detect the current fatigue status of a human participant, and the class detected was then passed from an OPC UA server to a personal computer (PC) with an OPC UA client. Such a connection would allow workers' fatigue status to be monitored continuously in real-time, and alarms would be raised if fatigue is detected for proactive health and safety assessment in smart factories.

1.3. Contributions

The first main contribution of this thesis is the proposed architecture that facilitates the transformation of legacy control systems to revolutionized ones. The proposed architecture requires minimal to no replacement of the existing operating legacy controllers. Hence, faster upgrade periods are achieved. The architecture was designed to be generic and non-exclusive to any specific application. To achieve that, open communication protocols as well as open software platforms were used. Also, the architecture allows for independent yet connected industrial processes, so system failure

or security breach damages can be mitigated. The architecture also enhances the integration of embedded devices, industrial controllers, cloud computation, and portable smart devices [26].

The second contribution is the development and validation of a mental fatigue detection system using a wearable PPG sensor. The proposed technique utilized the HRV features extracted from a commercial PPG sensor reading. The average HR for each participant was found to be comparable to its counterpart collected from an FDA-approved PPG sensor which validated sensor accuracy. In addition, a moving window algorithm was developed to automatically detect mental fatigue. Mental fatigue detection was performed using a Raspberry Pi controller with an OPC UA server, which were integrated with trained machine learning models and the moving window, which allowed for continuous monitoring. This study was submitted to the IEEE Access journal and is under review at the time this thesis was submitted.

1.4. Thesis Overview

This thesis is divided into the following four chapters: 1) Introduction, 2) Client/gateway Architecture, 3) Mental Fatigue Detection, and 4) Conclusions and Future Work. In Chapter 2, related literature about previously developed digital twin frameworks, as well as about the proposed architecture, a case study, and their results are presented. Chapter 3 includes a literature review on mental fatigue detection technologies as well as the study materials, design, results, discussion, and the connection with the architecture proposed in Chapter 2. Chapter 4 concludes the thesis and provides recommendations for future work related to the proposed architecture, as well as mental fatigue detection techniques.

Chapter 2.

Client/Gateway-Based Architecture

2.1. Literature Review

A digital twin is the evolution of virtual representation to accurately reflect the states of its physical equivalent [47]. A digital twin can be monitoring states of sensors and actuators installed on the physical system. The collected data is gathered on a local controller (e.g., PLC, Microcontroller, etc.). Then, the data can be forwarded to the digital twin via a multitude of communication protocols including OPC UA. The collected data can be stored and processed locally or forwarded to the cloud for further processing. Cloud platforms can facilitate further storage, big data processing, data mining, visualization, and applications of machine learning.

Leitão et al. [48] predicted that the OPC UA protocol will standardize multi-agent communication and solve multi-vendor compatibility challenges. They claimed that the protocol has the potential to be one of the key standards of Industry 4.0. OPC UA solves the data accessibility challenge between multi-vendor industrial controllers and their compatibility with various embedded devices since data and resources are accessible in the address space. Chen et al. [10] successfully used OPC UA to connect all compatible multi-vendor network nodes and to facilitate integration, troubleshooting, fault detection, and automatic correction.

Since the release of the OPC UA protocol, researchers have applied various architecture designs in different applications. Fernbach et al. [49] introduced a multi-agent architecture as a case study consisting of two layers of OPC UA servers. The first layer consisted of two portable OPC UA servers installed in different locations to monitor variables, and both servers reported data to an aggregating OPC UA cross-domain server in the second layer through a wireless area network (WAN). Haskamp et al. [50] presented a different architecture to upgrade traditional programmable logic controllers (PLCs) to be compatible with Industry 4.0 standards using the OPC UA protocol. Four PLCs were connected to dataFEED OPC Suite software, which acted as an OPC UA server. Variables were then published to Microsoft Azure cloud service. The data stored

on the cloud could then be fetched and displayed on a custom-designed graphical user interface (GUI).

Melo et al. [51] provided an architecture that complies with RAMI 4.0 architecture, and a case study on a FESTO MPS (Modular Production System) sorting station. The traditional Siemens PLC was replaced by a Raspberry Pi in the context of the physical controller, and TIA Portal with OpenPLC for the software. OpenPLC is an open-source development software that mimics PLC ladder diagrams, and it is mainly used for embedded controllers that employ C or Python, and simulation software. They ran both the OPC UA server and OpenPLC program on the Raspberry Pi and connected four OPC UA clients to the controller via Wi-Fi. The main drawback of such a system is the restrictions imposed by the controller on application flexibility. The migration process was also affected since a special external UniPi unit, which is an industrial IO connection board, was used for its compatibility with OpenPLC. Also, a dedicated application programming interface (API) was developed from scratch for RFID devices and added to the OpenPLC project since it was not supported by the software.

Tao and Zhang [52] presented an architecture for a virtual shop floor and used a Computer Numerical Control (CNC) machine to validate their model. They proposed a digital twin of the CNC machine using a computer aided design (CAD) model with added physical properties (e.g., cutting force, torque, and wear) and loads in order to predict faulty behaviors. Zhong et al. [53] developed an RFID-based system to create a digital twin to monitor and manage Keda Industrial Group’s mass-communication production shop floor.

Mizuya et al. [54] developed two approaches to build a digital twin of a Selective Compliance Assembly Robot Arm (SCARA). The first approach was to connect the robot to a Raspberry Pi, which had an OPC UA client with an MQTT publisher running on it. Meanwhile, Raspberry Pi was connected to a PC, which had an OPC UA server with an MQTT subscriber running on it. The second approach ran an OPC UA server on a PLC instead of a traditional PLC, while the MQTT subscriber remained in place but on a separate PC. Both approaches had two clients connected to the same server. However, a PLC in the second approach was used to control other manufacturing processes in addition to robot control.

Schleipen [55] established an OPC UA server-client connection to monitor and control a virtual industrial robot. They used a UA Sample server and a UA Sample client to monitor data and mimic the connection. On the visualization side, they used ProVis Visu software with 2D representation of a robot arm to represent the current positions and angles of the robot joints. In the context of digital twin creation using an online platform, Caiza et al. [56] introduced an architecture where they used AJAX, which is an HMI web programming platform, and ran it on a laptop as an OPC UA client. An OPC UA server was running on a Raspberry Pi and was connected to the first client. Siemens S7-1200 was connected to the server as the second client and was able to read and write tags of interest from/to the server.

Lastly, Ala-Laurinaho et al. [57] evaluated the feasibility of creating a digital twin on an online API called DataLink. They ran an OPC UA server on a Raspberry Pi to be able to control the overhead crane. The Raspberry Pi-API gateway was connected, which was GraphQL API in their case, to the crane via a switch. Although they implemented Raspberry Pi and connected it to the crane PLC successfully, the quality of the crane network was poor with a delayed response, according to them. The latency increased significantly as soon as multiple devices were connected to the gateway or large quantities of data were requested at the same time.

Langmann and Stiller [58] proposed an architecture for a server-based mixed mode (SMM) of PLC operations where runtime operations were taking place on the cloud to take advantage of server stability and to enable system monitoring by portable devices. Since their architecture removed physical controllers, which are used by the majority of production lines, process control algorithms have to be re-written on the cloud via an IoT or IIoT platform. In addition to the fact that this might delay the migration process from the physical controllers to the new system, since there is no online debugger to test and accurately simulate the code before operation, coding and runtime operations on the cloud are more susceptible to cyber-attacks. according to them. They employed the Node-Red platform, which has relatively fewer options for secure communication, data visualization, and connection to different platforms such as smartphones and tablets.

Some challenges were observed and reported in the literature. Those challenges include security concerns associated with internet cloud services [58], the lack of

integration of embedded controllers [21], [50], [55], lack of interoperability as various equipment that did not support OPC UA were used [21], [53], a slow upgrade process from the re-development and reconfiguration of control devices [51], [58], case specific frameworks that were only applicable to certain applications [10], [21], and complex frameworks as various communication protocols were used [54].

For example, Langmann and Stillar totally removed the traditional PLC and the control code had to be re-written to be executed on the cloud, which delayed the migration process due to compatibility issues and imposed various security concerns according to them. On the other side, Melo et al. [34] replaced the traditional PLC with a Raspberry Pi with OPC UA capabilities enabled. However, as the Raspberry Pi was not originally designed to act as an alternative to industrial controllers, external adapters and physical equipment, alongside developed software libraries, were added to the Raspberry Pi. As a result, the Raspberry Pi CPU utilization and temperature were significant and needed a heat sink according to them. Therefore, the Raspberry Pi was overloaded and was not able to perform any additional tasks.

Ala-Laurinaho et al. [57] and Mizuya et al. [54] connected embedded controllers with industrial controllers within the same network using OPC UA. However, they reported a significant delay in response time as the number of devices increased within their networks. Schleipen [55], Chen et al. [10], and Haskamp et al. [50] reported a lower latency in communication, but embedded controllers were not connected within their frameworks, which can significantly affect the delay as more devices are added to the network. As the latency increases, the real time monitoring and control aspect of the digital twin cannot be achieved, which results in an inaccurate representation of the physical counterpart.

2.2. The Proposed Architecture

Our proposed client/gateway-based architecture is achieved by connecting all OPC UA servers to a single client/gateway device. In addition to the gateway, every other device is considered a server node (i.e., acts as an OPC UA server). The architecture generally consists of server, gateway, cloud service, and end user nodes as depicted in Figure 2.1.

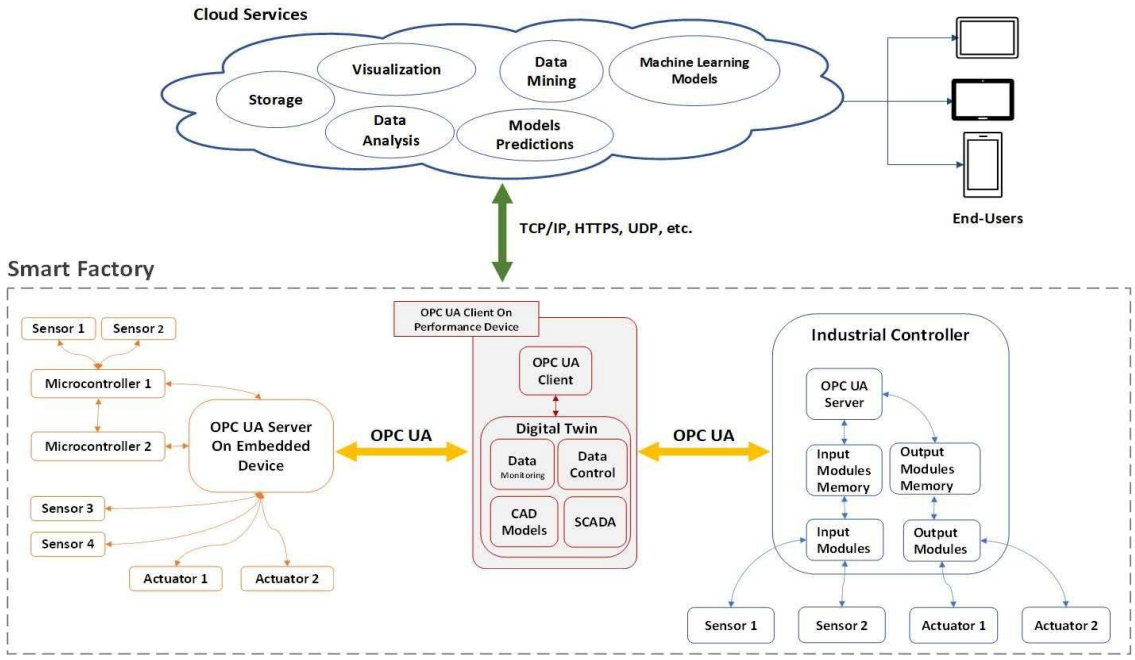

Figure 2.1. OPC UA client/gateway-based architecture in a smart factory.

2.2.1. Client/Gateway Node

The client/gateway node, shown in the center of Figure 2.1, acts as the point of intersection between three dissimilar but intersecting components: industrial controllers, embedded system controllers, and cloud services. One of the major benefits that the gateway offers lies in its capability of performing complex tasks and functions locally. The gateway in our architecture is a high-performance computer, Local Area Network (LAN) connectivity, and access to the cloud. As a result, the client/gateway can support

multiple digital twin platforms simultaneously. It can exchange data with common cloud platforms. As illustrated in Figure 2.1, the gateway reads data shared by OPC UA server nodes within the smart factory. Critical data processing is executed locally, before decisions are exchanged with other nodes, depending on the application. Further data processing performed by the gateway can also contribute to decreasing CPU utilization of servers.

2.2.2. Server Nodes

Server nodes are the controllers involved in different industrial processes. The controllers can be either industrial, such as of PLCs, or embedded, such as Raspberry Pi. Running an OPC UA server on every controller within the architecture has the following advantages.

- Data accessibility modes are set on the server end and restrictions on publishing specific data can be set.
- Prioritization of servers collecting critical data can be achieved by adjusting their publishing rate. Hence, received data can be scheduled accordingly.
- Redundancy of the system as failure of one server will not result in a full system failure. Failure of the gateway will result in disconnection from the cloud. However, individual server nodes can maintain local system control and status reporting.
- Replacement or reprogramming of a traditional PLC is not required for all devices with OPC UA compatibility.
- Process operations can be handled locally by the PLC instead of an online platform or an embedded system device such as Raspberry Pi.
- It enables cross-platform, multi-vendor integration between industrial and embedded controllers.

2.2.3. Cloud Services

Cloud services such as Microsoft Azure and Amazon Web Services (AWS) enable designers to utilize the full range of available functionalities, including machine learning algorithms, data storage, monitoring, and visualization. Cloud computing can also serve more sophisticated tasks such as coordinating full factory-level digital twins. A few common examples of cloud services, both over Internet and intranet, are illustrated at the top of Figure 2.1.

2.2.4. End-User Nodes

End-user nodes can include user-specific devices with access to the cloud. End users can access cloud services using available consumer electronics with network access and common web browsers. Specific application data can be exchanged with the cloud by accessing a secure webpage. Gateway users can be granted distinct levels of authorization depending on their respective roles in the process (e.g., machine operators, maintenance engineers, sales and marketing, data analysts, etc.). Utilizing modern consumer devices (e.g., smartphones and tablets) increases portability, and these can be easily upgraded without downtime on the factory floor. The use of these devices can augment the use of a stationary Human-Machine Interface (HMI) usually installed in close proximity to industrial equipment.

2.3. Application Case Study

2.3.1. Case Study: FESTO MPS

A FESTO MPS processing station, shown in Figure 2.2, was chosen to demonstrate the architecture and act as a proof-of-concept. A rotary indexing table delivers the disk-shaped part to multiple machining modules. The station has multiple inputs and outputs consisting of the rotary indexing table module, an electrical ejector solenoid, a geared DC motor, a testing (proofing) solenoid, and a drilling module with upper and lower limit switches. A Siemens S7-1516 was used to control process parameters. The PLC is connected to the gateway via Ethernet. The focus of the digital twin was solely visualization of the current position and angle of the rotating table that would reflect the state of the station. The primary rationale behind choosing the

processing station was the relatively fast rotary motion. The proposed architecture's performance can then be evaluated by seeing if the digital twin can reliably reflect the physical state of the system in real time.

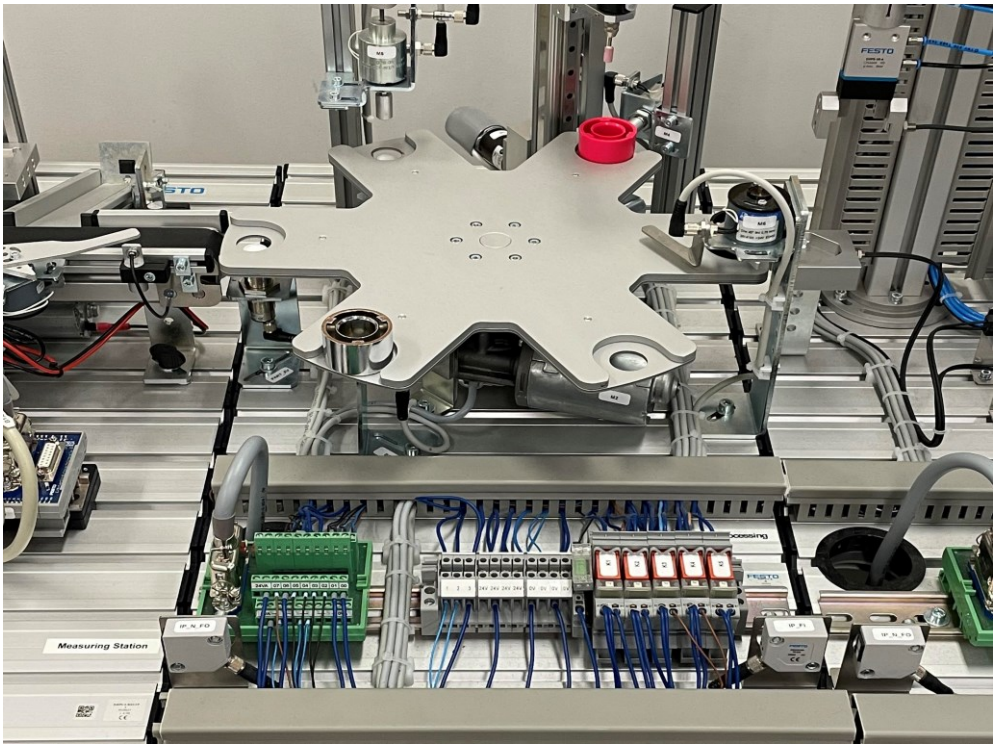

Figure 2.2. FESTO MPS Processing Station.

2.3.2. Case Study: Architecture

In the proposed architecture, a PC (e.g., laptop) acts as the gateway, while a PLC and an embedded system act as OPC UA servers. The embedded system consists of an Arduino Uno microcontroller board connected to a Raspberry-Pi single board computer. The Arduino Uno measures distance using an ultrasonic sensor and voltage through a potentiometer. The data is then transferred to the Raspberry Pi using the Universal Asynchronous Receiver Transmitter (UART) communication protocol. The Raspberry Pi serves as an OPC UA server and reports data to the client/gateway. The reported data from both servers is then merged and transferred to the gateway on the same LAN. The gateway computer has an HMI/SCADA platform (Ignition by Inductive Automation). Ignition Gateway operates as an OPC UA client and is connected to the

PLC and Raspberry Pi servers. The Ignition Designer module is then utilized to store data and create SCADA and HMI screens. Finally, two portable end-user devices, a smartphone and a tablet, are connected to the Ignition Designer module to monitor and control the data in real time. Figure 2.3 shows the case study architecture with all connections.

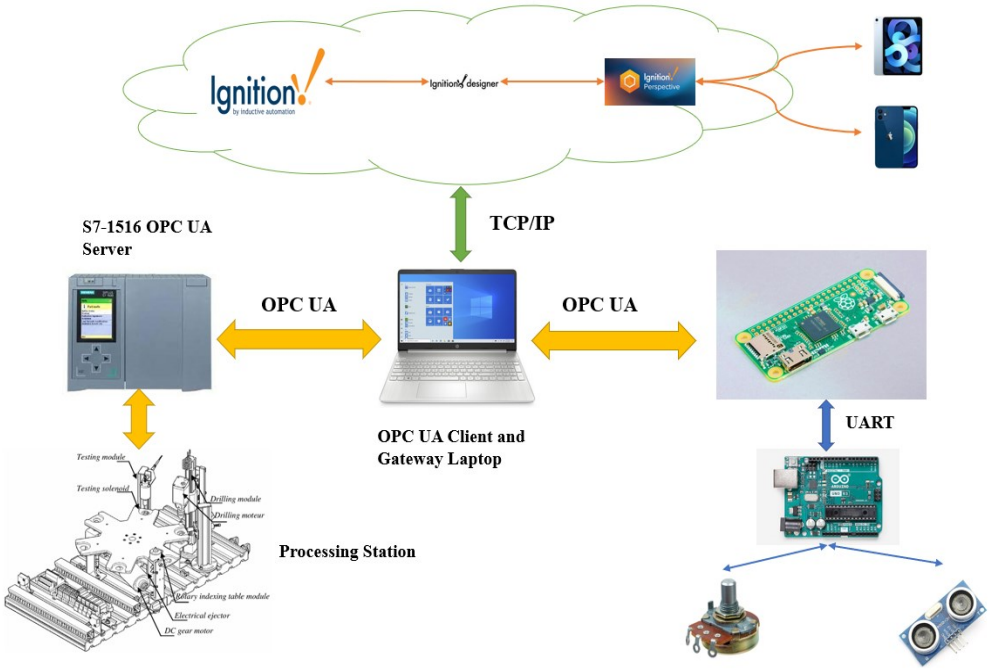

Figure 2.3. Case study architecture with Raspberry Pi and Siemens PLC running OPC UA servers.

2.3.3. Case Study: Server Nodes

The PLC OPC UA server addresses can be modified in relation to the existing PLC IP address. Originally, only the PLC was running the station's control program. Given correct access credentials, the gateway node was able to access all used input/output and memory tags on the server PLC. Properties of tags of interest can be modified and set to read and write or to read-only depending on the application. The sampling rate is the rate at which the OPC UA server polls the tag values from the controller, while the publishing rate is the rate at which the server publishes the tag values to all connected clients. The sampling rate was set to the shortest supported sampling period of 100 ms (i.e., 10 Hz), while the publishing rate was set to 200 ms (i.e., 5 Hz).

On the embedded system server node, the communication between the Raspberry Pi and Arduino Uno was done using UART at 9600 bits/s. The time-stamped sensor readings (distance and input voltage) were added to the same address space. A method similar to the one used by Melo et al. [32] was used to evaluate latency and CPU utilization. We chose to test an extreme scenario by connecting multiple OPC UA clients to the same server. Adding more clients will significantly increase the CPU utilization, as shown by Melo et al. [32]. Hence, portable devices were connected as clients to the server over a Wi-Fi network. A new OPC UA client was connected every 2 minutes over a total period of 6 minutes. After that, the Raspberry Pi CPU utilization, temperature, and latency were measured over the test period. A separate application to capture timestamps of the PLC and the Raspberry Pi was employed to evaluate the latency. Latency was calculated by subtracting timestamps at which the tag value changed at the source (i.e., Raspberry Pi) and the timestamp of the corresponding tag on the PLC end after synchronizing both system clocks.

2.3.4. Case Study: Gateway and Users Nodes

As mentioned above, a laptop running an OPC UA client acted as the gateway node. The gateway node was configured to facilitate secure data communication between servers and control user administrative privileges. Ideally, the gateway can communicate with cloud services and then to end users. In this research, the connection between the gateway and end users was done over intranet as a proof-of-concept.

A mobile application (Ignition Perspective) was installed on a smart phone to emulate an end user. Figure 2.4 illustrates the Ignition Perspective screen on the portable device. The HMI design was created using Ignition Designer and was only designed for real time visualization of the Processing Station and the Raspberry Pi readings, (i.e., no commands were sent from the screen to either device). The gateway polling rate was set to 50 ms (20 Hz), a sufficient rate to monitor the station in real time.

The data flow from portable devices to controllers is as follows: (1) when an interaction with the Ignition Perspective screen occurs, a change is reported to Ignition Designer, (2) Ignition Designer is connected to an Ignition Gateway from which all the tags are polled, (3) Ignition Gateway was running on a laptop and is connected to the Raspberry Pi using the OPC UA communication protocol; hence data were passed to

the Raspberry Pi. The communication between portable devices and the gateway is established via a secured Wi-Fi network. The gateway can be accessed from any browser using the gateway's IP address and port number.

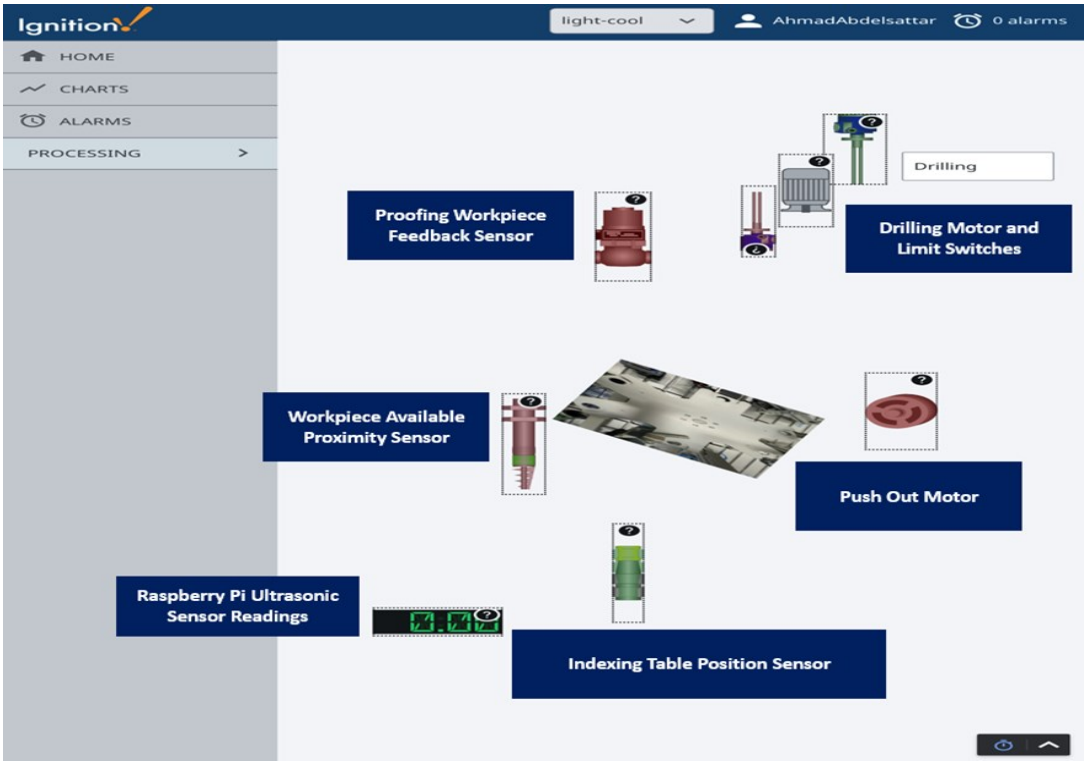

Figure 2.4. Ignition Perspective SCADA screen on a portable device.

2.4. Results

Although an OPC UA server/client communication was successfully established, its reliability should be tested on different devices to validate its efficacy. We performed a communication reliability test by connecting an additional OPC UA client API, which was UaExpert, to the processing station's PLC (i.e., one of the servers). A memory tag on the PLC was then modified according to the ultrasonic readings from the Raspberry Pi (the second server). UaExpert captures the source timestamp from the Raspberry Pi and the corresponding memory tag timestamp from the PLC and the difference will be calculated.

2.4.1. Latency Results

The PLC tags were updated at a rate of 4 Hz on UaExpert. This resulted in a maximum latency of 250 ms. OPC UA clients were connected every 2 minutes with the first client connected at the launch of the server. Due to the PLC server publishing limitations, values of tags were updated in the controller's memory at a faster rate than those of the OPC UA tag subscribers. Table 2.1 shows the differences between the tags' receiving and publishing times. The average difference for all readings was 0.110 ms with a standard deviation of 0.072 ms. The results show both consistency and scalability independent of the number of clients that are connected because the PLC and Raspberry Pi are publishing at a fixed scheduled time. As advanced data processing is handled by the gateway, fewer instructions will be performed by the Raspberry Pi allowing for faster program execution cycles. Hence, the client/gateway architecture contributes to decreasing the publishing rate of the server allowing for more accurate real-time communication.

Table 2.1. Servers Timestamps

Raspberry Pi Publishing Timestamp	PLC Server Publishing Timestamp	Difference (s)
2:56:30.853	2:56:31.017	0.164
2:59:33.708	2:59:33.767	0.059
3:00:13.870	3:00:14.017	0.147
3:00:56.104	3:00:56.267	0.163
3:01:30.250	3:01:30.267	0.017
3:01:54.424	3:01:54.517	0.093
3:02:12.502	3:02:12.517	0.015
3:02:48.683	3:02:48.767	0.084
3:03:04.770	3:03:05.017	0.247

2.4.2. Raspberry Pi CPU Usage and Temperature

The experimental results show a significant CPU utilization of the Raspberry Pi during the server launch as well as when connecting to the first client. CPU utilization showed a consistent increase whenever a new client connection was added to the server. However, the consistent utilization increase did not affect the latency as results show in the last sub-section. CPU temperature showed a maximum increase of approximately 2 ℃ above the nominal operating temperature at server launch and first client connection. Figure 2.5 shows the timeline for CPU utilization and temperature with impulses during new client connections and a consistent return to normal operating temperature after communication is established. Maintaining low operating temperatures is a consequence of the proposed architecture as operating temperatures are strongly correlated with CPU utilization that, in turn, is significantly reduced, since the Raspberry Pi is no longer tasked with high utilization processes.

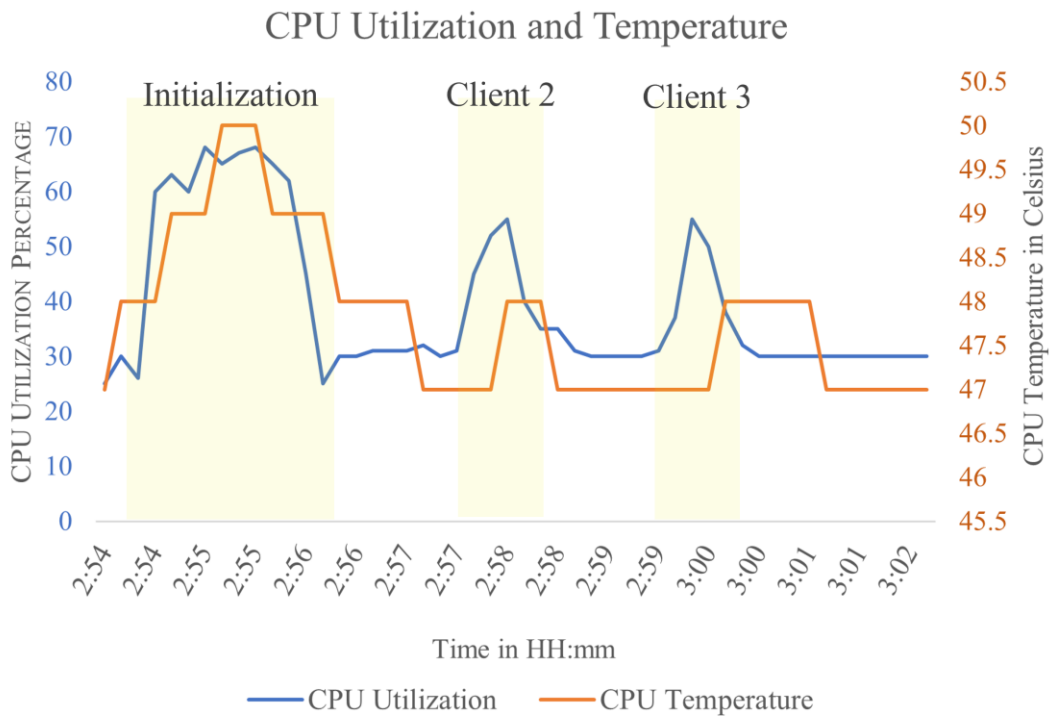

Figure 2.5. Raspberry Pi CPU usage and temperature while in operation. Spikes in the CPU usage and temperature occur upon establishing a new connection.

2.4.3. Limitations

During the configuration phase, the OPC UA server running on the PLC was limited by a minimum 5 Hz publishing rate. Similarly, the sampling rate was restricted to a minimum of 10 Hz. On the client side, the tag polling rate was set to 20 Hz. Another constraint was the lack of readily available visual components used to design HMI control screens. Ideally, 3D physical and dynamic models for the plant (i.e., the FESTO station) would adequately represent the digital twin.

2.5. Summary

In this chapter, the proposed client/gateway-based architecture was presented. The main contributions include showing the benefits of connecting an OPC UA Client to multiple servers simultaneously. As a proof-of-concept, an Arduino Uno was connected to a Raspberry Pi that ran an OPC UA server. On the other side of the network, a Siemens S7-1516 PLC also ran an OPC UA server. Both OPC UA servers, the Raspberry Pi and the Siemens PLC, were connected to the client/gateway laptop wirelessly (Raspberry Pi) and via an Ethernet cable (Siemens PLC).

The designed architecture was tested such that a new client was introduced to the Raspberry Pi OPC UA server every two minutes. The observed CPU utilization and core temperature only showed a substantial rise during initialization before returning to nominal steady state. Other minor utilization and temperature spikes were observed during the addition of new OPC UA clients.

In the next chapter mental fatigue is discussed as an application of the proposed Client/gateway architecture integrated with a human digital twin. Similar to the case study presented in this chapter, embedded sensors such as wearable HR sensors and microcontrollers such as Arduino Uno and Raspberry Pi were used to detect mental fatigue within the proposed smart factory concept.

Chapter 3.

Mental Fatigue Detection

3.1. Literature Review

In this section, pertinent works on mental fatigue detection are reviewed by dividing them into three physiological sensing categories: EEG, ECG. and PPG.

3.1.1. EEG

EEG is a test that allows brain activity signals to be recorded and monitored using metal electrodes and a conductive medium. Conventional non-invasive EEG sensors typically require a low-pass filter and a signal amplifier depending on the application [59]. The various frequency bands of EEG data are delta (0.5-4 Hz), theta (4-8 Hz), alpha (8-12 Hz), and beta (14-30 Hz). Changes in the power spectrum of the theta and alpha bands were reported to denote mental fatigue induced by a mental workload. For example, the power spectrum in the alpha frequency band decreased while performing cognitive tasks according to [60]. Also, a significant increase in the power spectrum of the theta band during sustained workload was observed in [61].

EEG is considered the gold standard for mental fatigue detection, where EEG electrodes are attached to the scalp. The direct contact with the scalp allows brain signals to be monitored. Hence, different patterns of brain activities during rest and fatigue mental states can be observed. Electrodes must be placed at specific locations on the scalp – called brain regions – to ensure stable signals. Those regions are standardized as the International 10-20 System for electrode placement [62]. As an example, Jain et al. [63] used a helmet-based EEG system with 8 electrodes to collect brain signals from various regions of interest (ROIs) to detect mental fatigue. EEG signals were transformed into sources using advanced matrix properties to extract meaningful features. Trejo et al. [64] followed a similar approach to detect mental fatigue using EEG. In their study, a Quik-Cap™ 32-electrode system and a Neuroscan Synamps™ 64-channel system were used to amplify brain signals. Although EEG

provides an accurate representation of brain activities, a few drawbacks exist including invasive and time-consuming installation as well as complex signal interpretation [65].

3.1.2. ECG

ECG graphs represent cardiac activities through measured electrical signals. Small metal plates known as electrodes are attached to the patient's skin. Electrodes gather signals to create the QRS complex. The QRS complex provides the essential information required for detecting heart rhythm and associated abnormalities [66]. Ten electrodes must be placed on several areas on the skin to collect electrical signals forming the QRS complex [67]. The variation of the electric potential in 12 directions is known as leads (three bipolar and nine monopolar). Bipolar leads signify electric potential between the right and left arms, called Lead I. Subsequently, the potential between the right arm and left foot is named Lead II, while the potential between the left arm and left foot is named Lead III. For monopolar leads, artificial reference points are established. These points are the left arm (aVL), the left foot (aVF), the right arm (aVR), and six chest electrodes, V1 to V6, with the right foot as a ground. Figure 3.1. shows the QRS complex, obtained with permission [68].

Figure 3.1. QRS complex for three consecutive heartbeats [48].

ECG has been investigated as a less complex alternative than EEG to detect mental fatigue. According to the literature, HRV features were used to accurately detect mental fatigue. HRV features consisted of time-domain and frequency-domain features to indicate the interference levels of the sympathetic nervous system (SNS) and parasympathetic nervous system (PSNS) [69]. Shaffer and Ginsberg [69] and Kim et al. [70] showed that PSNS and SNS regulate the heart activities at rest and under stress conditions, respectively. A number of features particularly strongly correlated with PSNS activation including the number of interval differences of successive normal-to-normal intervals (NNI) greater than 50 ms (NNI_50), the proportion of NNI_50 to the total NNI (pNNI_50), and high frequency (HF) [71].

Huang et al. [24] showed the feasibility of mental fatigue detection using a wearable ECG sensor, “LaPatch” from Texas Instruments. In time-domain, the mean value of NNI decreased, indicating a faster HR during the mental fatigue state. In frequency-domain, low frequency (LF), high frequency (HF), as well as the ratio between them (LF/HF) all increased in the fatigue state compared to the non-fatigue (i.e., rest) state. The highest classification accuracy obtained was 75.5% using the k-nearest neighbour (KNN) machine learning model. He et al. [72] showed that mental fatigue is detectable from HRV features extracted by a convolutional neural network (CNN). The CNN deep learning algorithm was applied to a 10-second ECG reading time frame, which allows for a real-time detection. Tsunoda et al. [73] also demonstrated that ECG-based HRV features could be affected by mental fatigue. ECG signals were collected during an Advanced Trail Making Test (ATMT) of 45 male participants. Their results showed an accuracy of 84.4% for detecting cognitive fatigue using the Support Vector Machine (SVM) algorithm.

Based on previous works, HRV features such as mean NNI and LF/HF ratio have been proven as an effective and efficient ECG-based mental fatigue detection tool. Despite continuous improvements in the implementation and accuracy of wearable ECG devices [74], [75], challenges in terms of users’ comfort and relatively complex setup still exist as explained in [67], [76]. Those drawbacks have led to further research into the association between PPG and ECG in order to extract similar HRV features from PPG readings.

3.1.3. PPG

PPG technology uses light reflection to detect changes in blood volume in the microvasculature. PPG sensors consist of a light emitter and a receiver that use near-infrared light wavelength. PPG sensors are traditionally placed on a fingertip or an earlobe as signal amplitude is less noisy and less invasive compared to other locations [77]. Hence, light intensity fluctuations resulting from changes in blood volume can be captured by the receiver [78]. One drawback is that PPG sensors are highly influenced by motion-induced noises since PPG sensors use light intensity to detect blood volume [77], [79], [80].

PPG sensors are increasingly widely being adopted in both research-grade and commercial wearable devices. In 2009, Lu et al. [78] proved that HRV features can be extracted using PPG and compared the results with ECG. PPG was employed in this study for the following reasons [81], [82]: (i) HRV features are extractable and highly comparable to ECG counterparts, (ii) implementation simplicity and users' level of convenience and comfort, and (iii) significantly lower cost compared to ECG devices.

As previously discussed, PPG can be effectively used to generate HRV features leading to a classification result highly comparable to ECG [78]. The correlation between SNS and PSNS with heart rhythm patterns presented by HRV features was demonstrated in [69], [70]. This pilot study shows that wearable PPG sensors are sufficient for providing an accurate detection of mental fatigue. An experiment was conducted to measure mental fatigue levels of 11 volunteer participants using a PPG sensor. The experimental setup and protocol are discussed in the following section.

3.2. Study Materials and Methods

3.2.1. Participants

In total, 11 volunteer participants were recruited for this study: 5 males and 6 females, with a mean age of 25.8 years and a standard deviation of 3.28 years. The study was approved by SFU Research Ethics Board (REB), and all participants submitted their informed consent. As part of the exclusion criteria, any participants who had recent mental or cardiac disorders were excluded from the study, similar to [24],

[72]. Participants who reported having overwork-related conditions were also excluded as transient state (between rest and fatigue) changes over time [24].

3.2.2. Hardware and Software

An off-the-shelf wearable PPG sensor (DFRobot Gravity) was used in this study as shown in Figure 3.2A. Sensor data was read using an Arduino Uno microcontroller board, then forwarded to a host PC. Sensor data was then stored in a text file before conversion to a Comma Separated Values (CSV) file. This particular PPG sensor was chosen for the study for the following reasons. Firstly, the sensor has built-in signal noise filtering. Secondly, its compact size (28×24 mm) makes it convenient for subjects to wear with a Velcro strap. Thirdly, its reliability and usability have been shown in previous research studies. For instance, Liao et al. [83] used the same sensor in their experiment to monitor physiological sleep signals. It was also utilized to measure HRs of participants during intense physical activities in [84], [85]. In our study, in order to validate the sensor's accuracy, a comparison against the FDA-approved wireless VitalStream™ continuous hemodynamic vital signs monitor (Caretaker Medical®, USA) was performed. Figure 3.3 shows a 3-second sample of the recorded PPG readings collected by the DFRobot sensor for a participant showing the peak detection algorithm results. Differences in duration between successive peaks were used to extract all HRV features in time and frequency-domains.

The Psychomotor Vigilance Test (PVT) used in this study was originally developed by NASA to measure reaction time and the difference between rest and fatigue reaction times [86], [87]. In addition, an Advanced Trail Making Test (ATMT) was utilized as the mental workload. Mizuno et al. demonstrated that ATMT can be utilized to induce mental fatigue [88], [89]. The PVT and ATMT were installed as mobile applications on a tablet. Both tests are shown in Figure 3.2B and Figure 3.2C, respectively.

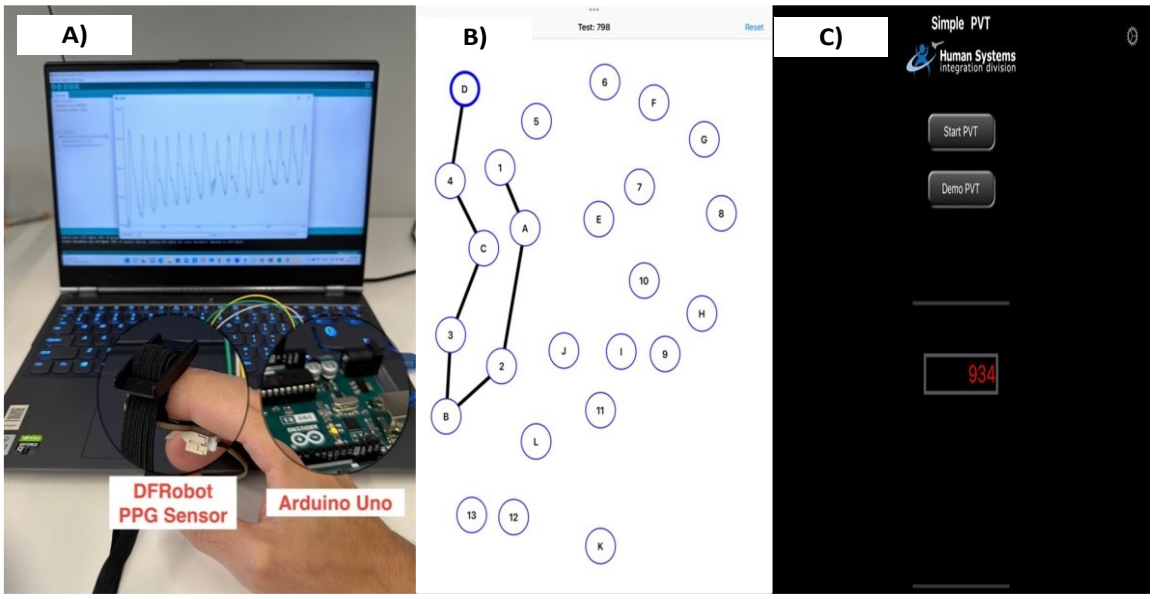

Figure 3.2. **A) PPG sensor attached to the index finger, which is connected to the Arduino Uno. B) Advanced Trail Making Test session running on a commercial tablet. C) NASA Psychomotor Vigilance Test session with a reaction timer (in ms) shown in the bottom box.**

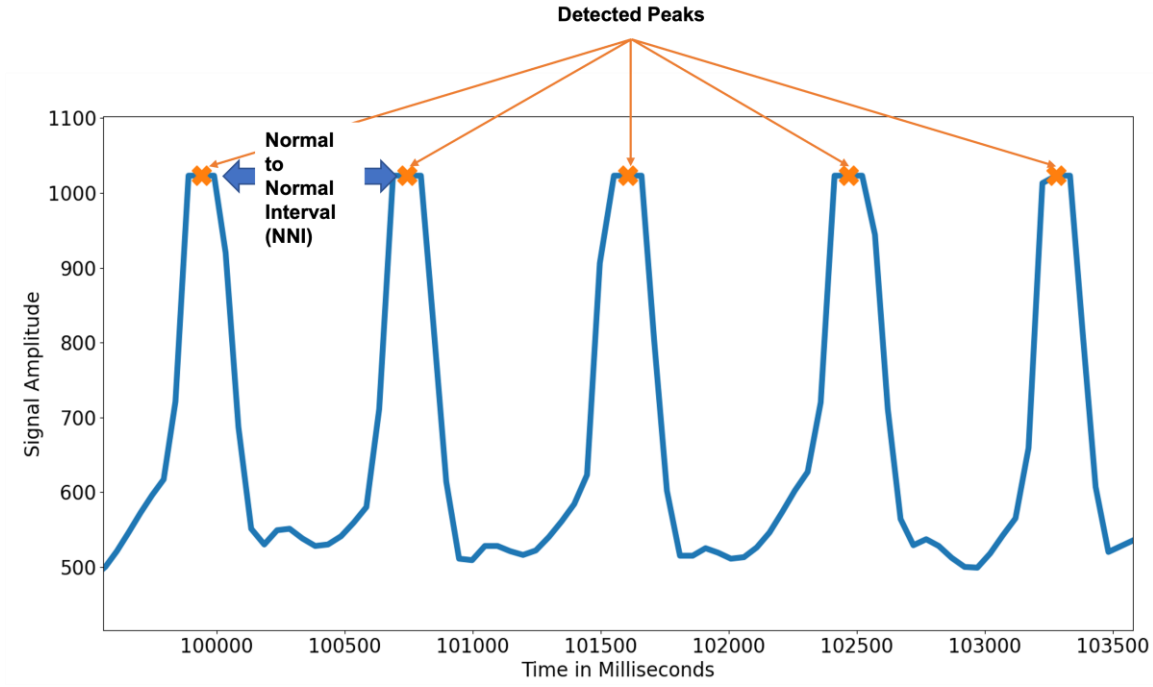

Figure 3.3. **Three seconds of PPG readings with peaks detected.**

3.2.3. Experimental Design

The time of the experiment was chosen by participants to ensure they were in a rested (non-fatigued) state. The participants were asked not to consume caffeinated drinks, alcohol, or medication that may affect their concentration or attention level at least two hours before the experiment [90], [91]. At the start of the experiment, each participant was asked to fill in the Chalder Fatigue Scale (CFS) questionnaire [24], [92]. The questionnaire consisted of 14 survey items with answers on a 1-5 scale (lowest 1 indicates least fatigue, highest 5 indicates most fatigue) as shown in Table 3.1. The CFS questionnaire provides a self-reported numerical indication of the participants' fatigue levels. After concluding the questionnaire, PPG readings, PVT, and ATMT were performed.

Next, the participants were asked to perform the PVT to measure their resting reaction time. Upon completion, they were asked to perform the ATMT for a duration between 20 and 40 minutes, depending on the time at which mental fatigue state was self-reported by the participants. After that, PPG readings were again collected for an additional 10 minutes before repeating the PVT to measure their reaction time in fatigue state. At the conclusion of the experiment, each participant was asked to complete the CFS questionnaire again for comparison with the rest state results. The timeline of the experiment is illustrated in Figure 3.4. The participants performed the experiment in a sitting position with the chair adjusted to their comfort level.

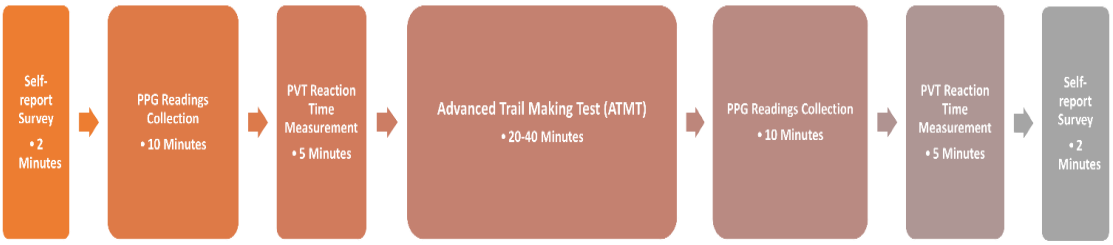

Figure 3.4. Experiment timeline starting with self-report questionnaire at rest state and ending with a second round of the survey at fatigue state.

Table 3.1. Chalder Fatigue Scale Questionnaire

Item	Description	Scale
1	Do you have any problems with tiredness now?	1-5
2	Do you need to rest more now?	1-5
3	Do you feel sleepy now?	1-5
4	Do you have problems starting things now?	1-5
5	Do you start things without difficulty but get weak as you go on now?	1-5
6	Are you lacking in energy now?	1-5
7	Do you have less strength in your muscles now?	1-5
8	Do you feel weak now?	1-5
9	Do you have difficulties concentrating now?	1-5
10	Do you have problems thinking clearly now?	1-5
11	Do you make slips of tongue when speaking now?	1-5
12	Do you find it more difficult to find the correct word now?	1-5
13	How is your memory now?	1-5
14	Have you lost interest in the things you used to do now?	1-5

3.2.4. Data Preprocessing

PPG signals were collected using the wearable sensor placed on a participant's finger of choice, with the index finger as the recommendation [83]. HRV features in both time and frequency-domains were extracted using the Python programming language [93]. A few prominent features in the time-domain were selected, including the mean of NNI (Mean_NNI), the standard deviation of HR (Std_HR), the number of interval differences of successive NNI greater than 50 ms (NNI_50), and pNNI_50. The selected time-domain features are further discussed in Sec. IV. Other time-domain features include standard deviation of normal-to-normal (SDNN), root mean square of successive differences between normal heartbeats (RMSSD), standard deviation of successive normal-to-normal interval differences (SDSD), the number of interval differences of successive NNI greater than 20 ms (NNI_20), and pNNI_20. In the frequency-domain, low frequency bands (LF) from 0.04 Hz to 0.15 Hz, high frequency bands (HF) from 0.15 Hz to 0.4 Hz, and the ratio between them (LF/HF) were analyzed where $f(\lambda)$ is the power spectrum.

According to Huang et al. [24], since the sampling frequency was fixed at 250 Hz, PPG recordings should last at least 10 cycles of the lowest frequency (e.g., 0.04 Hz) to accommodate it. A single cycle at 0.04 Hz takes approximately 25 seconds and 10 cycles take 4.16 minutes to complete. The HRV features were extracted from 10-minute PPG intervals instead of 5-minute intervals used in [93] to increase the robustness and resilience of the readings [94]. HRV features were also analysed using the HRV analysis Python library. Formulas used to obtain time and frequency-domain HRV features were as follows:

$$SDNN = \sqrt{\frac{1}{n-1}\sum_{i=1}^{n}(NN_i - NN_{mean})} \quad (1)$$

where SDNN is highly correlated with SNS and PSNS activity in longer recording periods, and it is measured in ms. SDNN is considered the gold standard to detect cardiac risks when monitored in longer periods, typically over 24 hours [69].

$$RMSSD = \sqrt{\frac{1}{n-1}\sum_{i=1}^{n-1}(NN_{(i+1)} - NN_i)^2} \quad (2)$$

where RMSSD indicates the variation of HR and is highly correlated with the PSNS activity compared to SDNN. Similar to SDNN, recordings over 24 hours are related to pNN50 and HF [69].

$$Mean\_NNI = \frac{1}{n}\sum_{i=1}^{n} NN_i \quad (3)$$

where Mean_NNI is calculated by summing all NNI within a time frame and dividing them by the number of intervals. The Mean_NNI is measure in ms and is used to calculate Mean_HR. Large values of Mean_NNI indicate slower Mean_HR and vice versa.

$$Mean\_HR = \frac{60*1000}{NN_{mean}} \quad (4)$$

where Mean_HR is calculated by dividing 60,000 by the Mean_NNI to convert from ms to beats per minute (bpm). Generally, slower Mean_HR indicates minimum physical or mental activity and faster Mean_HR indicates more physical or mental activity. Rest HR over 90 bpm is correlated with higher risks of cardiac failure [95].

$$SDSD = \sqrt{\frac{1}{n-1}\sum_{i=1}^{n}(|NN_i - NN_{i+1}| - NNdif_{mean})^2} \quad (5)$$

where SDSD was found to efficiently represent short-term HRV as reported in [69]. McNames and Aboy [96] showed a high correlation between SDSD, RMSSD, and HF, which can be used to determine the level of PSNS interference in regulating heartbeats.

$$NNdif_{mean} = \frac{1}{n-1}\sum_{i=1}^{n-1}(|NN_i - NN_{i+1}|) \quad (6)$$

where the mean difference of consecutive NNI is called $NNdif_{mean}$ and is used to calculate SDSD.

$$\sum_{i=1}^{n}\begin{cases} NNI\_50 = NNI\_50 + 1, & |NN_{i+1} - NN_i| > 50\,ms \\ NNI\_50 = NNI\_50, & |NN_{i+1} - NN_i| < 50\,ms \end{cases} \quad (7)$$

where the number of consecutive intervals in which the difference in NNI duration is over 50 ms is called NNI_50. According to the literature, lower NNI_50 counts are highly interconnected with the activation of SNS and deactivation of PSNS and vice versa [45], [69].

$$\sum_{i=1}^{n}\begin{cases} NNI\_20 = NNI\_20 + 1, & |NN_{i+1} - NN_i| > 20\,ms \\ NNI\_20 = NNI\_20, & |NN_{i+1} - NN_i| < 20\,ms \end{cases} \quad (8)$$

where the number of consecutive intervals in which the difference in NNI duration is over 20 ms is called NNI_20. Similar to NNI_50, lower NNI_20 counts are highly interconnected with the activation of SNS and deactivation of PSNS and vice versa [45], [69].

$$pNNI\_50 = \frac{NNI\_50}{N} * 100 \quad (9)$$

where the proportion of NNI_50 to the total number of intervals during a time frame is called pNNI_50. This metric indicates the level of interference of PSNS in regulating heartbeats, similar to NNI_50. If the pNNI_50 value is significant, it denotes PSNS activation. Hence, the rest state can be identified and vice versa [45], [69].

$$pNNI\_20 = \frac{NNI\_20}{N} * 100 \quad (10)$$

where the proportion of NNI_20 to the total number of intervals during a time frame is called pNNI_20. This metric indicates the level of interference of PSNS in regulating heartbeats, similar to NNI_20. If the pNNI_20 value is significant, it denotes PSNS activation. Hence, the rest state can be identified and vice versa [45], [69].

$$Range\_NNI = Maximum\ NNI - Minimum\ NNI \tag{11}$$

where Range_NNI is calculated by obtaining the difference between the maximum and minimum values of NNI during a specific time frame. In general, a large Range_NNI value indicates significant differences between heartbeat intervals, which can be interpreted as high HRV (i.e., rest state) and vice versa.

$$Std\_HR = \sqrt{\frac{\sum_{i=1}^{n}(HR - Mean\_HR)^2}{n-1}} \tag{12}$$

where Std_HR measures the deviation in HR within a specified time frame. Higher Std_HR values indicate variation within heartbeat intervals, which denotes PSNS dominance or rest state.

$$Median\_NNI = \begin{cases} NN\left[\frac{n}{2}\right], & n\ is\ even \\ \frac{\left(NN\left[\frac{n-1}{2}\right] + NN\left[\frac{n+1}{2}\right]\right)}{2}, & n\ is\ odd \end{cases} \tag{13}$$

where, similar to Mean_NNI, Median_NNI is measured in ms. Large Median_NNI values indicate slower Mean_HR and vice versa.

$$Max\_HR = \begin{cases} HR_n > HR_{n-1}, & Max\_HR = HR_n \\ HR_n < HR_{n-1}, & Max\_HR = HR_{n-1} \end{cases} \tag{14}$$

$$Min\_HR = \begin{cases} HR_n > HR_{n-1}, & Min\_HR = HR_{n-1} \\ HR_n < HR_{n-1}, & Min\_HR = HR_n \end{cases} \tag{15}$$

where Max_HR represents the highest heart rate interval obtained within a specific time frame. On the other hand, Min_HR represents the lowest heart rate obtained within a specific time frame. Both features are measured in bpm.

$$HF = \int_{0.15}^{0.40} f(\lambda) d\lambda \tag{16}$$

where the HF or the respiratory band frequency ranges from 0.15 Hz to 0.4 Hz and the result unit is ms^2. The HF reflects the PSNS activity in regulating the heart activity based on the respiration cycles. Normally, heartbeats accelerate during inhalation and decelerate during exhalation. As HF is correlated with both pNNI_50 and RMSSD, high HF levels indicate PSNS activation, detecting the presence or absence of mental fatigue. To calculate HF, a minimum data recording of one minute is required [45], [69].

$$LF = \int_{0.04}^{0.15} f(\lambda) d\lambda \tag{17}$$

where the LF frequency ranges from 0.04 Hz to 0.15 Hz and the result unit is ms^2. The LF reflects both SNS and PSNS activities in regulating the heart activity, primarily SNS. Therefore, lower LF values indicate SNS activation, hence mental fatigue and vice versa. To calculate LF, a minimum data recording of two minutes is required [45], [69].

$$LF/HF = \frac{\int_{0.04}^{0.15} f(\lambda) d\lambda}{\int_{0.15}^{0.40} f(\lambda) d\lambda} \tag{18}$$

where LF/HF indicates the extent to which SNS and PSNS are regulating heart activities. Generally, a low LF/HF denotes that PSNS is dominant in the context of regulating heartbeats, which indicates rest state, whereas a high LF/HF indicates SNS dominance, which implies mental fatigue [45], [97].

$$VLF = \int_{0.0033}^{0.04} f(\lambda) d\lambda \tag{19}$$

where the very low frequency (VLF) power spectrum ranges from 0.0033 Hz to 0.04 Hz and the result unit is ms^2. According to Pham et al. [97] and Bouzida et al. [98], VLF is highly associated with body temperature regulation and vasomotor activities.

$$LFnu = \frac{LF}{(LF+HF+VLF)} \tag{20}$$

where the normalized value of LF is calculated by dividing the LF power spectrum by the total power spectrum of the recorded data. Similar to LF, LFnu is highly correlated with the activation of SNS, which indicates a mental fatigue state [99]. As SNS interference in regulating heartbeats becomes more significant, LFnu increases.

$$HFnu = \frac{HF}{(LF+HF+VLF)} \tag{21}$$

where the normalized value of HF is calculated by dividing the HF power spectrum by the total power spectrum of the recorded data. Similar to HF, HFnu is highly correlated with the activation of PSNS, which indicates a mental rest state [99]. As PSNS interference in regulating heartbeats becomes more significant, HFnu increases.

3.3. Results

3.3.1. Feature Selection

In this section, HRV features with the highest correlation with the classification output were selected based on a p-value significance test. The statistically significant HRV features are listed in Table 3.2. Performing a statistical analysis on the dataset allowed the use of reduced-order machine learning models. The objective of the feature selection step was to eliminate HRV features that do not significantly indicate different mental states. P-value significance testing was used to select the most salient HRV features. The HRV analysis library generated 16 time-domain features and 7 frequency-domain features. The HRV features with the lowest p-value scores, with the significance level α set to 0.05, were retained for further calculations.

Table 3.2 shows the selected HRV features. Eight of these features were used in [65] and four of them in [24]. One advantage of keeping the number of features as low as possible was to decrease the CPU utilization required to classify an unknown sample. This approach will significantly affect power consumption and improve feasibility for real time monitoring using wearable devices. Also, irrelevant features can negatively affect classifiers' weights and accuracy. The Gini index was used to perform importance evaluation, in addition to significance testing [45], [100]. A decrease in Gini index indicates the purity of the node in the random forest feature selection. A higher Gini index of a feature increases its contribution to the output. Table 3.3 shows the Gini index as well as ANOVA scores for HRV features. Features with the highest Gini index were passed to machine learning models for additional noise filtering as suggested by [45]. The Pearson correlation coefficients were calculated for the mean and median NNI, as well as between mean and maximum HR due to their correlation [69]. Median_NNI had a Pearson's *r* value of -0.982, and -0.821 for the mean and maximum HR, respectively;

and 0.995 for the Mean_NNI. This indicated high positive and negative linear correlations. Hence, Median_NNI was selected due to its higher Gini index and correlation with the remaining features. The overall feature selection process is illustrated as a flow chart in Figure 3.5, resulting in the following four features being selected: NNI_20, NNI_50, Std_HR, and Median_NNI.

Table 3.2. Statistically Significant HRV Parameters

Number	Description	Rest State Mean	Fatigue State Mean	P-Value
1	**NNI_20:** Number of interval differences of successive NN-intervals greater than 20 ms.	513.91	466.09	0.00062
2	**NNI_50:** Number of interval differences of successive NN-intervals greater than 50 ms.	283.55	231	0.00085
3	**Std_HR:** Standard deviation of heart rate.	7.28	5.96	0.0116
4	**Mean_NNI:** The mean of NN-intervals.	790.55	827.08	0.0170
5	**Mean_HR:** The mean Heart Rate.	77.53	73.87	0.0195
6	**Median_NNI:** Median absolute values of the successive differences between the NN-intervals.	792.59	828.36	0.0249
7	**Max_HR:** Maximum value for heart rate.	109.44	100.03	0.0479

Table 3.3. Gini Index and ANOVA Scores For Statistically Significant Features

Feature Order	Description	Gini Index	ANOVA
1	NNI_50	0.130	3.795
2	Std_HR	0.121	2.398
3	NNI_20	0.085	3.281
4	Median_NNI	0.079	0.702
5	Mean_NNI	0.060	0.801
6	Mean_HR	0.024	0.956
7	Max_HR	0.017	0.912

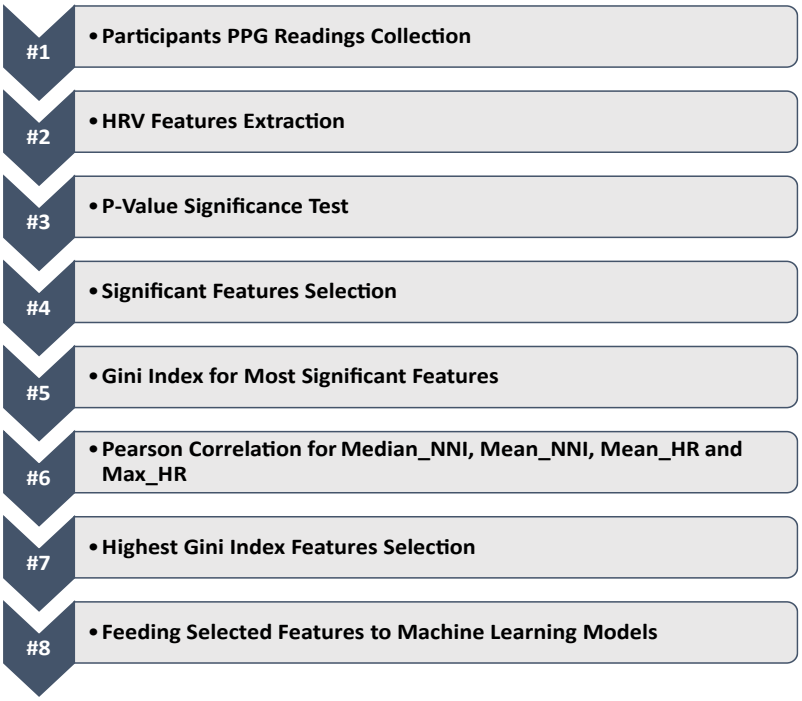

Figure 3.5. Flowchart of the proposed feature selection process from the collection of participants' data to feeding extracted HRV features into the machine learning models.

Figure 3.6 shows the difference in NNI durations between the rest state and the fatigue state for a participant. The plot shows the first 40 HR intervals, which correspond to approximately 30 seconds of PPG readings. A noticeable difference between the two states can be clearly observed. The red color represents the NNI duration after the experiment (i.e., mental fatigue state), while the blue color represents the NNI duration at rest. The Mean_NNI for the participant was 719.91 ms at rest and 814.59 ms after the test, denoting a slower HR in the fatigue condition. Consequently, this participant's HRs were 84.34 and 74.36 bpm, at rest and fatigue, respectively.

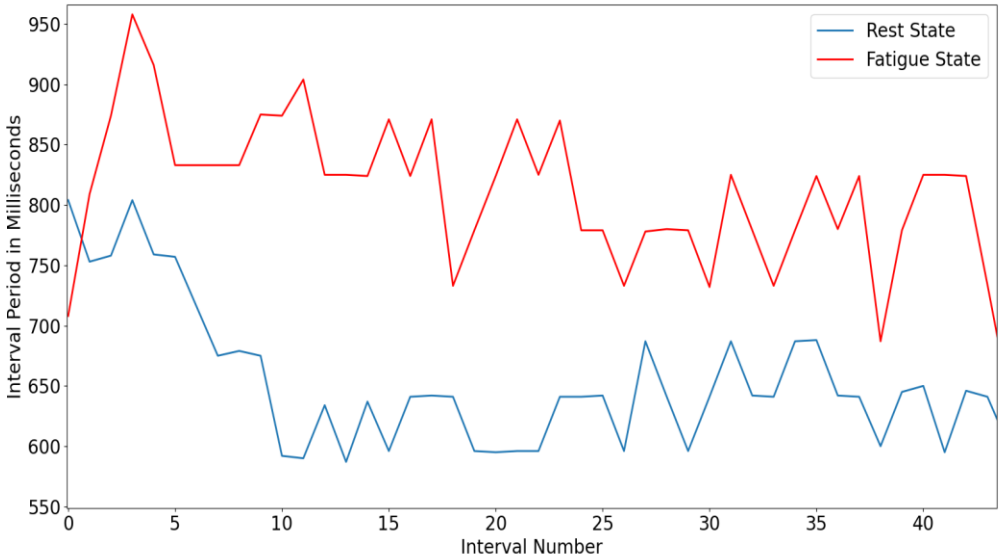

Figure 3.6. NNI durations for a participant at rest and fatigue states for the first 40 intervals which approximately correspond to the first 30 seconds.

3.3.2. Machine Learning Classifiers

The machine learning models (classifiers) evaluated in this study were Logistic Regression (LR), Artificial Neural Network (ANN), Support Vector Machine (SVM), Decision Tree (DT), Random Forest (RF), K-Nearest Neighbor (KNN), Stochastic Gradient Descent (SGD), Naïve Bayes (NB), and Extreme Gradient Boosting (XGBoost). These models were used in previous studies and were proven to detect mental fatigue effectively [45], [65], [101].

The machine learning hyperparameters were tuned using the GridSearchCV tool provided in the Scikit learn library to obtain the optimum hyperparameters values. Classifiers' hyperparameters were as follows:

- LR (penalty: L1, C: 10)
- ANN (activation function: ReLu, number of nodes: 256, number of hidden layers: 5)
- SGD (loss: squared hinge, penalty: L1)
- SVM (C:1, kernel: RBF)
- DT (min_samples_leaf: 5, max_depth: 100)
- RF (no _estimators: 30, min_samples_split: 4)
- XGBoost (lambda: 2, n_estimators: 500, max_depth: 10)
- NB (priors: None, var_smoothing: 1e-09)
- KNN (n_neighbors: 4, weights: uniform)

The available dataset was divided into a 70% training set and a 30% test set. Several coefficients were calculated including classification accuracy (CA), precision, recall, and F1 score to evaluate model performance. Coefficient parameters were true positives (TP), true negatives (TN), false positives (FP), and false negatives (FN). All coefficients were calculated in compliance with the 10 k-fold cross-validation to increase model reliability and robustness. The formulas used were calculated in compliance with the 10 k-fold cross-validation technique, which added more reliability and confidence to the results. Formulas used to calculate the coefficients are shown in equations (13) through (16):

$$\text{CA} = \frac{TP+TN}{TP+TN+FP+FN} \tag{22}$$

$$\text{Precision} = \frac{TP}{TP+FP} \tag{23}$$

$$\text{Recall} = \frac{TP}{TP + FN} \quad (24)$$

$$\text{F1} = 2 * \frac{Precision * Recall}{Precision + Recall} \quad (25)$$

Table 3.4. Comparison of Machine Learning Classifiers' Performance

Model	CA %	F1	Precision %	Recall %
ANN	**93.8**	**0.937**	**94.4**	**93.8**
LR	**93.8**	**0.937**	**94.4**	**93.8**
SGD	**93.8**	**0.937**	**94.4**	**93.8**
SVM	87.5	0.875	90.0	87.5
Tree	87.5	0.875	87.5	87.5
RF	81.2	0.812	81.7	81.2
XGBoost	81.2	0.812	81.7	81.2
NB	81.2	0.812	81.7	81.2
KNN	75.0	0.746	76.7	75.0

3.3.3. Automatic Detection via a Moving Window

To incorporate the proposed mental fatigue detection method in wearable devices, a moving window was implemented. The moving window automatically detects mental status based on the HRV features extracted from the most recent 10 minutes of PPG readings, with a 1-minute increment between successive rolling windows.

As a proof-of-concept demonstration, an additional healthy participant (22 years old, female) was recruited. The participant was asked to wear the PPG sensor and to remain as static as possible as PPG readings were recorded for the total duration of the experiment. To eliminate the need for an extended duration of the experiment and the participants' inconvenience associated with the extended period, the PVT was utilized as the alternative mental workload. The PVT is a mentally demanding test that showed effectiveness in inducing mental fatigue in shorter periods, typically between 10 and 20 minutes [102] compared to the 20~40 minutes reported by the participants using the ATMT. In the literature, the PVT was the sole mental workload used in [103], [104], and was combined with a driving simulator in [105]. In our experiment, the PVT started after collecting 10 minutes of PPG readings at rest. The participant self-reported mental fatigue after 11 minutes into the PVT, at which point the test was terminated. PPG readings were recorded continuously for an additional 10 minutes. Figure 3.7 shows the results of the moving window with LR, ANN, NB, and KNN. LR and ANN were the models that showed the best accuracies (in Table 3.4), whereas the last model (KNN) was included for comparison purposes. The LR, ANN, and NB models showed different mental fatigue thresholds, while the KNN model showed a fluctuation in the prediction. The fluctuation occurred between the 25^{th} and 27^{th} minutes, meaning further investigation and optimization are required before this particular classifier can be utilized. The fatigue state stabilized at around 29 minutes for the KNN model, which was only two minutes before data recording had been completed. Varying thresholds for the machine learning models depend highly on fine tuning of the models' hyperparameters, which were optimized using the GridSearchCV method. NB detected mental fatigue at around 5 minutes before mental fatigue had been reported by the participant. ANN detected mental fatigue at around 2 minutes before actual mental fatigue had been reported by the participant, and then the PVT was concluded. LR detected mental fatigue at 22 minutes, which was 1 minute after mental fatigue was reported by the participant. For this particular case study and the models' hyperparameters, ANN outperformed all other classifiers in terms of the speed of mental fatigue detection and accuracy. NB showed a better performance than LR and KNN in terms of the speed of mental fatigue detection.

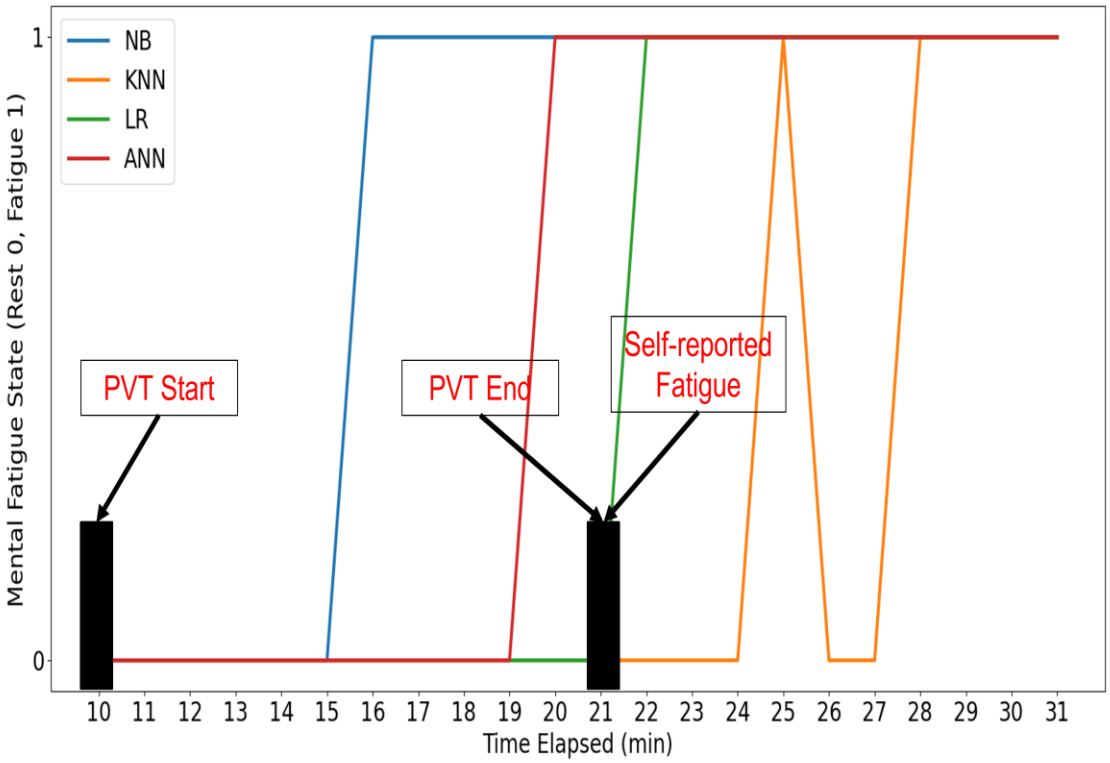

Figure 3.7. Automatic fatigue detection via moving window using LR, ANN, NB, and KNN machine learning models.

3.4. Discussion

3.4.1. Main Findings

Mental fatigue was predicted using HRV features obtained from an off-the-shelf PPG sensor, with a resulting accuracy comparable to ECG sensors used in similar studies [45], [72]. SGD, ANN, and LR were found to be the best classifiers with an accuracy of 93.8%. Results from all classifiers are listed in Table 3.4.

Several HRV features that contribute to differentiating between mental states were identified. NNI_50 and NNI_20 had the most significant influence on the classifiers. NNI_50 and NNI_20 indicate the extent to which the SNS and PSNS are involved with heartbeat regulation [69], [101]. The results show that the NNI_50 and NNI_20 values were significantly greater before the ATMT test than afterwards. This indicates more HR variation, PSNS dominance, and, in-turn, a mental rest state.

After the ATMT test, the NNI_20 and NNI_50 values were significantly lower for each participant, indicating more consistent heartbeats. This implies the SNS was dominant in regulating the heartbeats, indicating a mental fatigue state. Figure 3.8A shows the NNI_20 count of all participants, while Figure 3.8B shows the comparison of the NNI_20 count between males and females at both mental states. All participants experienced a significantly lower NNI_20 count at the fatigue state compared to rest state, except for participant 10 as shown in Figure 3.8. Box plots for the most significant features for both genders can be found in Appendix C. Also, the complete ANOVA calculations for both genders at both mental states can be found in Appendix D.

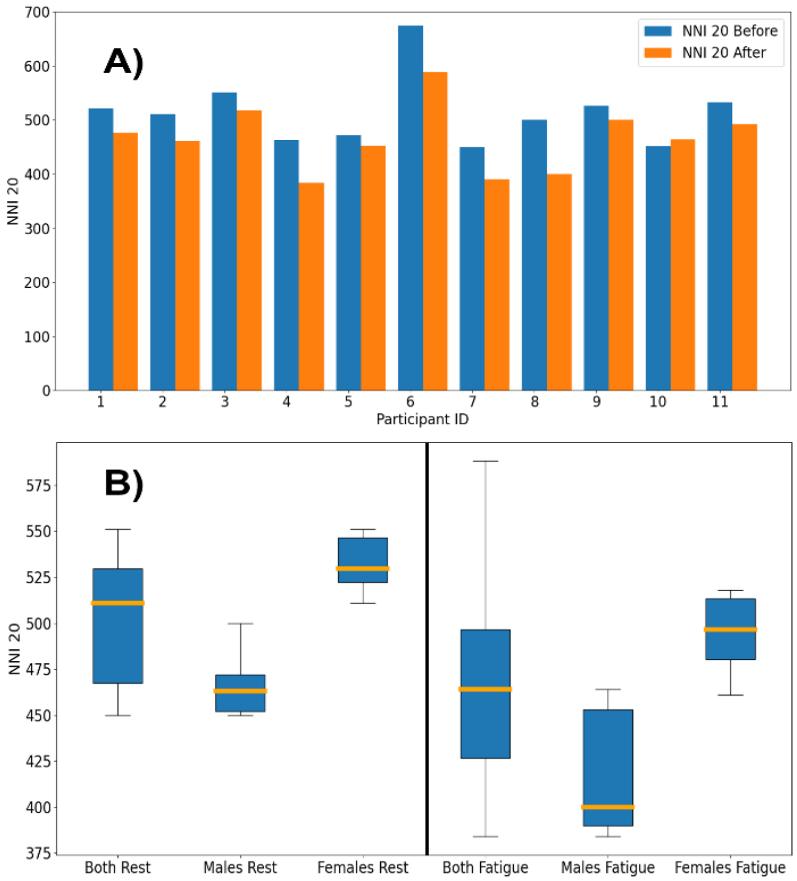

Figure 3.8. A) NNI_20 count for all participants with the blue bar representing the rest state and the orange bar representing the fatigue state. B) Box plot showing the difference in NNI_20 between males and females at rest state (left side) versus fatigue state (right side) with the orange bar representing the median.

Similar to the NNI_20 and NNI_50 values, Std_HR followed the same trend. As shown in Table 3.2, the mean value of Std_HR was 7.29 bpm at rest and 5.96 bpm at fatigue states, indicating a more significant deviation in HR when the participants were at rest. The Median_NNI value increased from 792.59 ms at rest to 828.26 ms at fatigue, which implies a drop of HR. The complete HRV parameters for all participants before and after the experiment can be found in Appendix E.

Furthermore, the PVT results supported the above HRV results that indicated a significant difference between the fatigue and non-fatigue mental states. Figure 3.9A shows the participants' mean reaction times obtained from the NASA PVT application, while Figure 3.9B shows the differences between the two mental states as well as between males and females in both states. The figure shows a significant difference in reaction time between the two states, the p-value was 0.00035. The mean reaction time was 337.64 ms at rest and 465.55 ms at the fatigue state.

It is noticeable that female participants had a generally higher NNI_20 count at the rest state, compared to males. This observation was also true at the fatigue state over a significantly narrower range compared to males. The mean Std_HR at the rest state was 8.425 bpm for females compared to 5.901 bpm for males, indicating more variability in HR for females in the rest state.

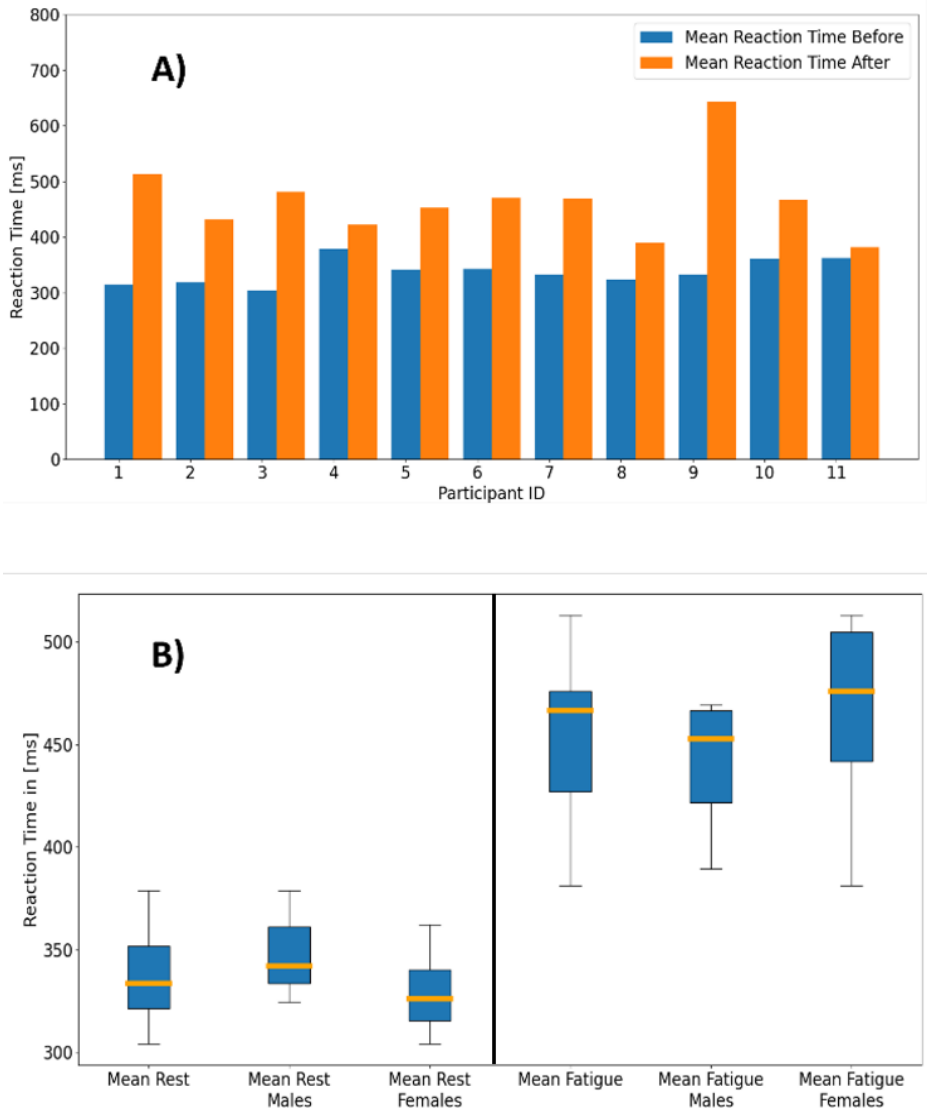

Figure 3.9. **A) The reaction times of all participants with the blue bar representing the rest state and the orange bar representing the fatigue state. B) Box plot showing the difference in reaction time between males and females at rest state (left side) versus fatigue (right side) with the orange bar representing the median.**

As mentioned before, a comparison between the DFRobot PPG sensor and the FDA-approved VitalStream™ was performed. According to VitalStream's datasheet, the device is capable of detecting NNI with an accuracy up to 6 ms between peaks. To compare both sensors, data were recorded simultaneously for a period of two minutes, and then the HR was analyzed. Regarding the results, the mean HR for all participants

obtained from VitalStream™ was 72.477 bpm, while the mean was 73.103 bpm for the DFRobot PPG sensor with a p-value of 0.30475 (i.e., no significant difference) and a mean square error (MSE) of 2.259 bpm. Table 3.5 shows the detailed error calculations for both sensors. However, the table only shows seven participants out of 11 due to data corruption of either one of the sensors during the recordings. Hence, four participants' data were excluded. Figure 3.10 shows the VitalStream sensor displaying the HR and the blood pressure using the finger cuff attached to a participants' finger.

Table 3.5. VitalStream Vs DFRobot Error Comparison

Participant Number	VitalStream	DFRobot	Error %
1	76.53	76.82	0.3775
2	77.31	79.21	2.3987
3	78.66	87.59	3.5852
4	68.22	69.42	1.7591
5	80.57	80.41	0.1990
6	N/A	N/A	N/A
7	59.66	58.26	2.4030
8	N/A	N/A	N/A
9	N/A	N/A	N/A
10	66.39	66.02	0.5624
11	N/A	N/A	N/A

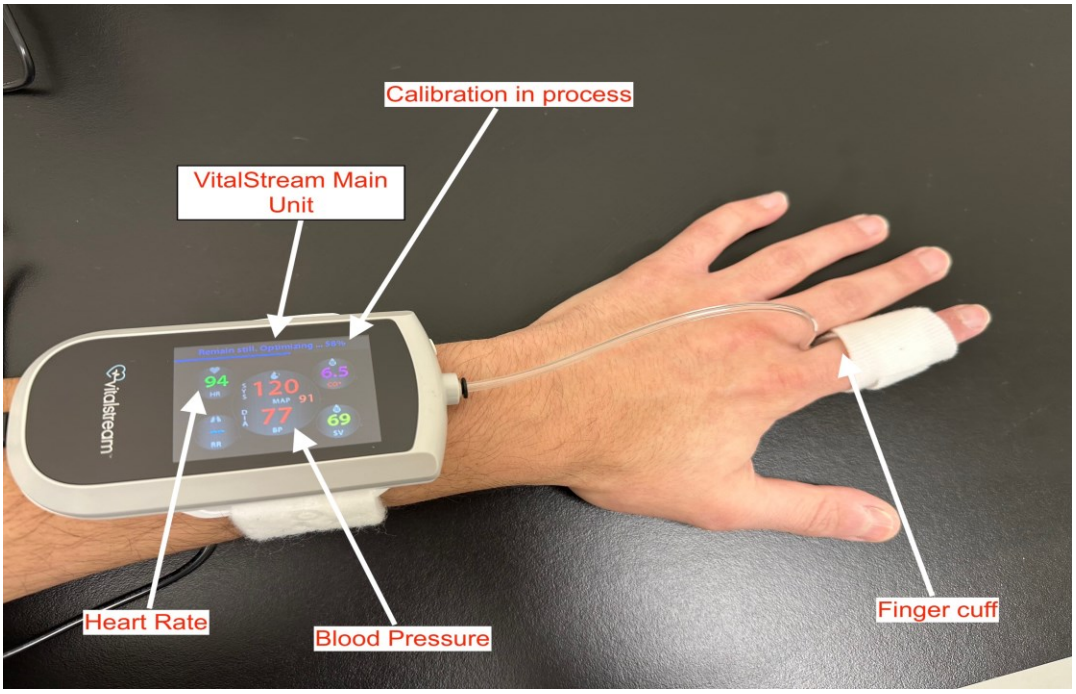

Figure 3.10. VitalStream device in the calibration mode.

3.4.2. Comparison with Relevant Work

The results show that the NNI_20 and NNI_50 counts significantly dropped due to the activation of SNS. This aligns with the ECG-based work of Huang et al. [45], where pNNI_50 was lower in the mental fatigue state compared to the non-fatigue (or rest) state. Std_HR in the mental fatigue state was lower than the non-fatigue state, a similar result obtained by Yue et al. [101]. Median_NNI increased and the HR decreased at the fatigue state aligning with results obtained in [91] and [106].

Frequency-domain features were excluded in this study based on the significance testing for feature selection. For instance, Huang et al. [45] obtained higher LF, HF, and LF/HF ratio in the fatigue state compared to the non-fatigue state, whereas those features decreased in [101] and [90].

Multiple features are required to obtain a higher classification accuracy. Huang et al. [45] obtained the highest accuracy when Mean_NNI, pNNI_50, total power (TP), and LF were combined and fed into the classifiers. In our study, the proposed combination of features (NNI_20, NNI_50, Std_HR, and Median_NNI) was accomplished through a

multiple stage feature selection process by employing p-value and Gini index scores to eliminate any irrelevant features.

3.4.3. Limitations and Proposed Solutions

The relatively small number of participants was the main limitation in this pilot study. It is recommended that future studies recruit a higher number of participants. Participants were mainly young healthy individuals with no reported chronic health challenges or mental disabilities. Participants from different backgrounds as well as different age groups will be considered in our future study. In addition, this study utilized ATMT as a mental stressor to induce mental fatigue within a controlled short period, 60 to 80 minutes for the entire experiment. A longer duration should be considered in further studies to emulate typical workplace environments (e.g., eight hours).

Consistently attaching an off-the-shelf PPG sensor to participants proved to be a challenge. Participants were asked to refrain from movement to the best of their abilities to minimize motion-induced data inaccuracies. This can be inconvenient for long-term experiments or continuous monitoring for extended periods of time. Attaching sensors to the wrist is recommended. A comparative study between PPG sensor locations (e.g., index fingers and wrist) should be further investigated. Lastly, a customized compact casing can be designed and manufactured to facilitate the sensor placement and minimize motion-induced noises.

3.5. Application Case Study: A Connection with The Proposed Client/Gateway Architecture

3.5.1. Integration within Smart Factory

As previously mentioned, the developed client/gateway architecture enables the connection of microcontrollers with industrial controllers. In the previous case study mentioned in Chapter 2.3, a potentiometer and an ultrasound sensor were connected to an Arduino Uno and then an OPC UA server (Raspberry Pi). In the current case study, the PPG sensor replaced the ultrasound and the potentiometer. Since the developed moving window algorithm (Chapter 3.3.3), the machine learning classifiers, and the OPC UA server were programmed in Python, they were all integrated and deployed to the

Raspberry Pi. After the connection between the OPC UA server and the main OPC UA client/gateway had been established, the machine learning classifiers' decisions were reported to the client/gateway. Hence, a human digital twin unit was effectively created to simulate the monitoring of a worker's mental fatigue state. Figure 3.11 shows the updated proof-of-concept architecture on the right side of the figure as the left side (the machine digital twin) has already been evaluated in Chapter 2.3. When the machine learning classifier indicated a mental fatigue state, an alarm would be raised on the Alarms screen of the Ignition Perspective interface (see Figure 3.12). The blue color indicates acknowledged alarms, while the red color indicates active unacknowledged alarms. In real-life scenarios, Ignition Perspective provides an option to acknowledge alarms only with a comment to ensure those alarms have been properly addressed.

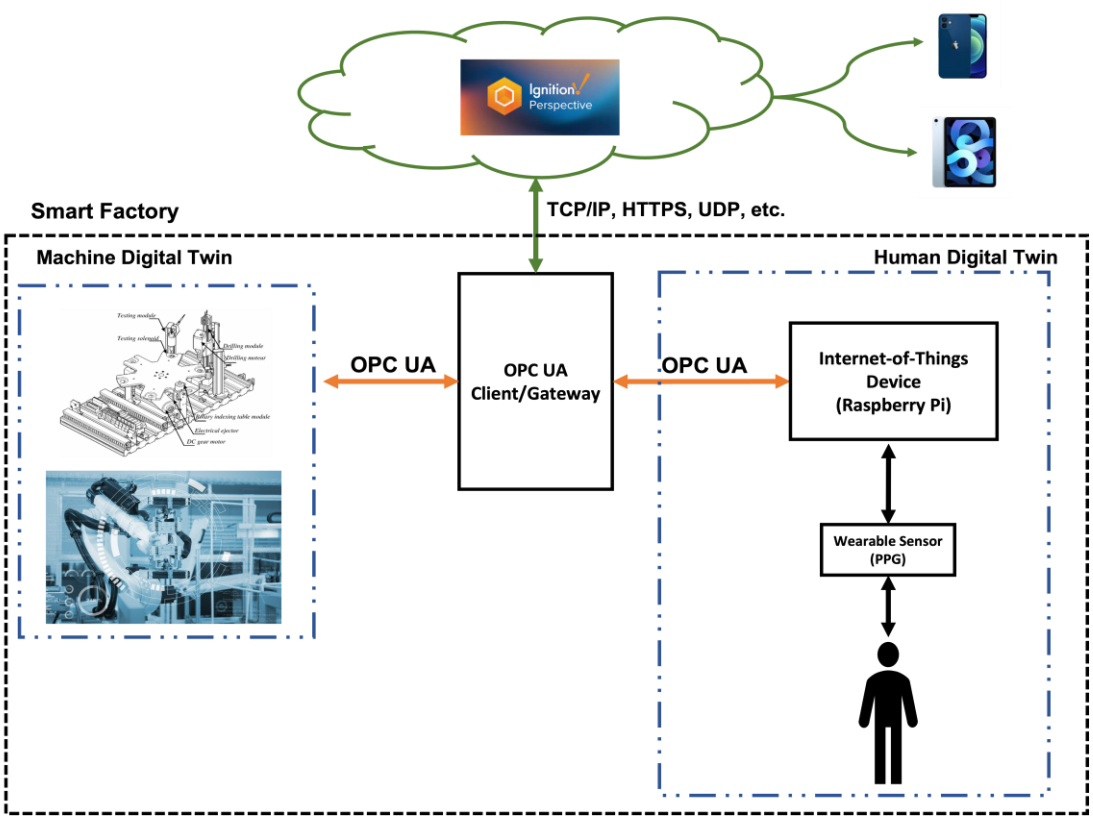

Figure 3.11. Human digital twin unit to monitor mental fatigue status.

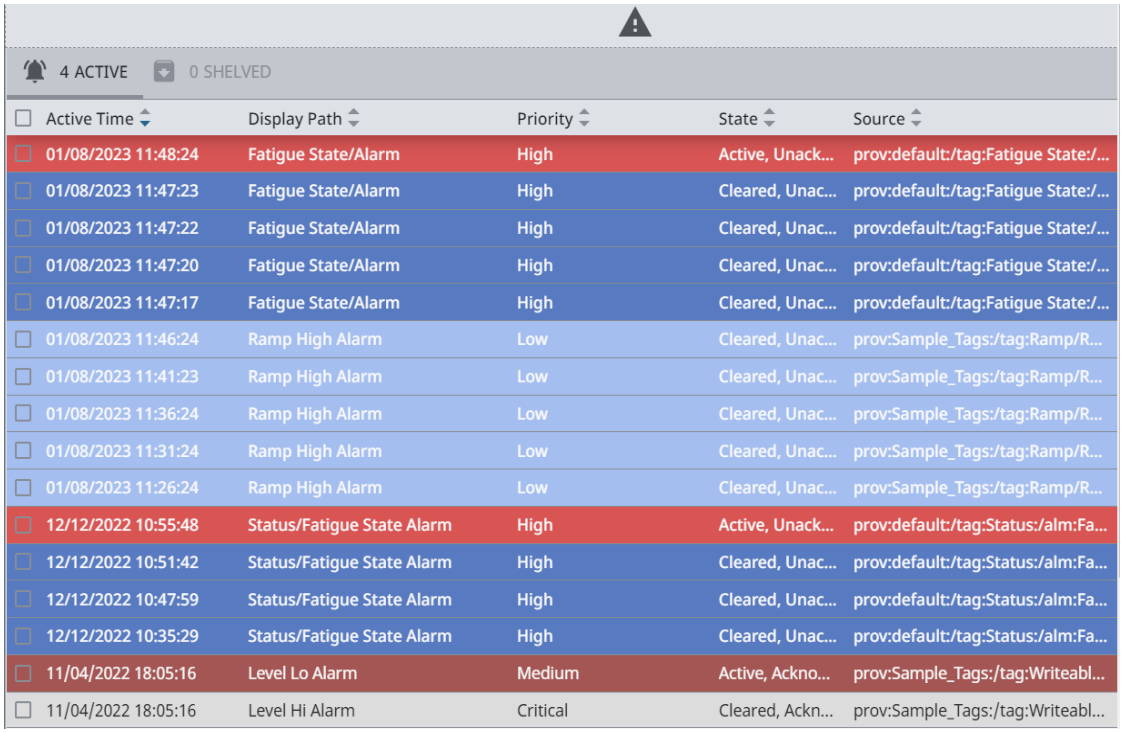

Figure 3.12. The alarm screen on Ignition Perspective.

3.5.2. Raspberry Pi CPU Utilization and Temperature

The Raspberry Pi CPU utilization and temperature were recorded similarly to Chapter 2.4.2 while running the algorithm. The ANN model was deployed to the Raspberry Pi and a simulation was performed using 31 minutes of pre-recorded PPG readings. As a proof-of-concept, the moving window was moving at a rolling rate of one minute of PPG readings per program loop. The processing speed remained constant as the code length and Raspberry Pi clock frequency remained unchanged.

The initialization phase consisted of OPC UA server initialization and data and classifier loading. During each iteration, the moving window extracted the last 10 minutes of PPG recordings, preprocessed them, and then the ANN classifier predicted the mental state. Subsequently, the ANN prediction was passed to the OPC UA server and published to all OPC UA clients connected (e.g., using Ignition). The classifier's prediction along with publishing to the OPC UA server resulted in spikes as can be observed in Figure 3.13. During the initialization phase, the CPU utilization peaked to

80%, followed by an expected increase in temperature, which, in turn, gradually increased and peaked at 44 °C. Then CPU utilization and temperature dropped to approximately 45% and 42 °C, respectively.

In conclusion, the Raspberry Pi CPU utilization remained approximately 45% with some minor spikes. Hence, the Raspberry Pi was not overloaded. Also, CPU temperature remained within the idle range, which is 40 to 50 °C, throughout the simulation, which can be considered as average power consumption. The Raspberry Pi CPU utilization and temperature are demonstrated in Figure 3.13.

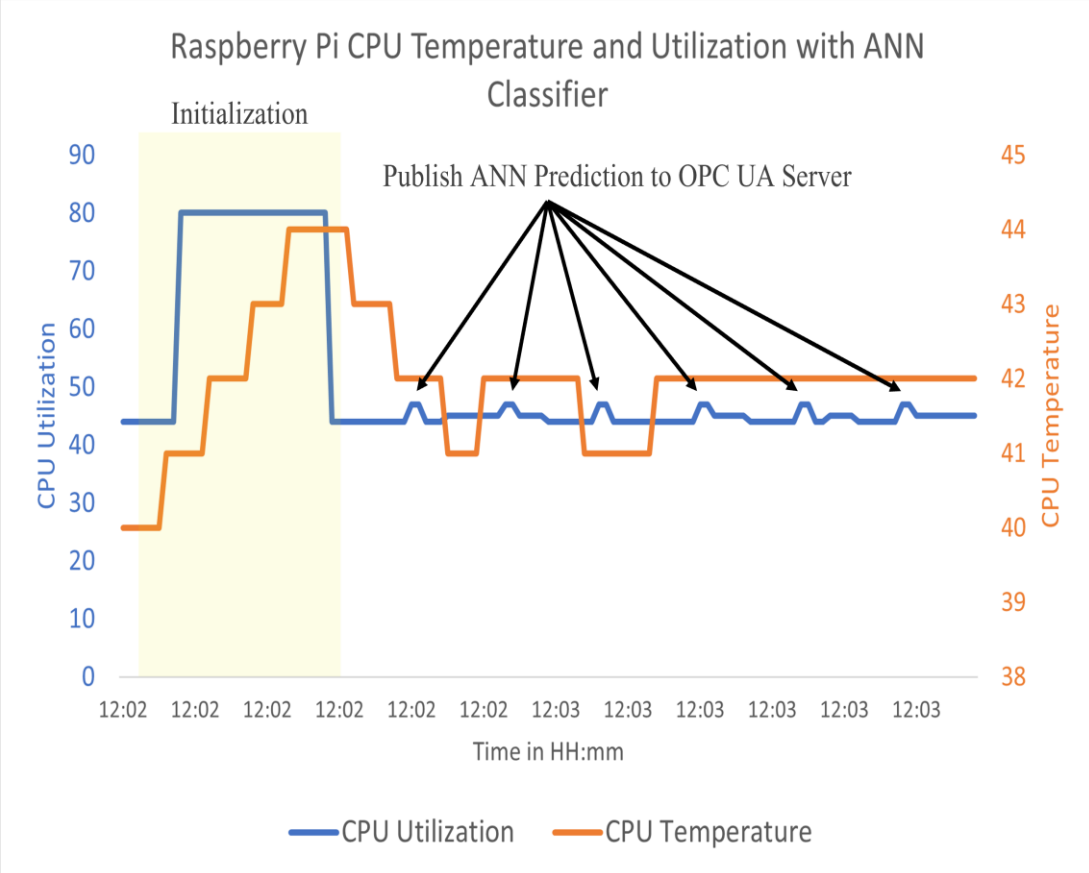

Figure 3.13 Raspberry Pi CPU Temperature and Utilization with ANN Classifier. The CPU utilization is presented by the blue color and the temperature is represented by the orange color.

3.5.3. Potential Real-Life Implementation Scenarios

As explained earlier, mental fatigue can have serious repercussions on workers' safety. Fang et al. [107] studied the effects of mental fatigue on construction workers. In their pilot study, 20 construction workers were recruited and split into two groups (A and B) with different tasks assigned to induce mental fatigue in a controlled environment. Results showed a significant increase in the number of errors committed by each worker with an increase from 6.4 to 9.9 mistakes per worker in Group A, and 4.5 to 6.9 mistakes in Group B. The study concluded that early detection of mental fatigue can potentially decrease the risk of errors on a construction site and prevent injuries. In the previous case, mental fatigue detection can be employed to the construction workers to detect mental fatigue and trigger alarms to supervisors to take preventative measures.

Bowen et al. [108] conducted a survey of quality and process control technicians in the forestry industry (a lumber mill plant) in New Zealand. The study concluded that both mental and physical fatigue adversely affect the reaction time of workers, which was correlated with a significantly higher injury risk and accident probability. In this case, our algorithm can trigger alarms within the SCADA system of the plant and perform emergency stops to specific segments of the plant if required.

3.6. Summary

In this chapter, mental fatigue detection using PPG technology was presented. The technique involved the extraction of HRV parameters from PPG readings and various calculation were performed. An experiment was performed on 11 healthy human subjects without any recent mental or cardiac conditions. All participants performed the experiment within 60-80 minutes until mental fatigue was reported by the participant. To provide a numeric basis for different mental fatigue states, a PVT application developed by NASA was utilized to measure the participants' reaction time before and after the experiment. To select the relevant features, a statistical significance test using p-value was performed. Then Gini index and ANOVA tests were performed on the statistically significant features resulting from the first step. The final features selected were: NNI_20, NNI_50, Std_HR, and Median_NNI.

The selected features were used to train the machine learning models to detect mental fatigue. The highest obtained accuracy on any machine learning classifiers were LR, ANN, and SGD with an accuracy of 93.8%. Also, an additional healthy participant was recruited to perform the experiment with the PPG sensor recording during the entire duration of their session. The machine learning classifiers were then integrated with an automatic moving window for automatic fatigue detection. The results indicated different thresholds for the machine learning classifiers, which was expected as all models' hyperparameters were set to default. Subsequently, the developed machine learning models and the automatic moving window were integrated within the proposed client/gateway architecture. A case study of a mental fatigue alarm on Ignition Perspective was presented, which was triggered whenever a mental fatigue state had been detected.

Chapter 4.

Conclusions

4.1. Conclusions

This thesis proposes a smart factory concept in which digital twin units are constructed for machines and workers. In our proposed concept, machine and worker digital twin units are all interconnected forming the overall shop floor digital twin. This concept leverages the advancements in both Industry 4.0 and Operator 4.0 by connecting wearable devices that monitor health conditions with machines in the shop floor via an OPC UA client/gateway-based architecture. In our demonstrated case study, the health condition of interest was the worker's mental fatigue, in order to mitigate safety risks. To integrate the wearable IoT (used in Operator 4.0) with IIoT devices (used in Industry 4.0), a new data exchange architecture was developed along with a novel mental fatigue detection technique.

The first part of this work proposed and evaluated an OPC UA client/gateway-based architecture on a FESTO MPS Processing Station. The proposed architecture simplified system connectivity while reducing the computation cost of process controllers by utilizing a gateway device for more demanding processing tasks. The main contributions of this work can be summarized as follows:

- Creation of HMI screens with digital twin capabilities (real-time visualization) for existing systems without modification of existing PLC programs.
- Enabling user-nodes (e.g., portable devices) to locally or remotely monitor and control processes through secure connections.
- Low latency communications between industrial and embedded controllers.
- Decreasing CPU utilization on embedded controllers (e.g., Raspberry Pi) and, in turn, core temperature. This decreases power consumption, especially for battery-powered applications.

Cross-platform protocols such as OPC UA allow communication between multi-vendor devices. This facilitates the design of smart factories and provides designers additional

flexibility in choosing system components. Our research directions include (i) the integration of wearable devices for monitoring workplace safety, data storage, and processing on available cloud platforms; and (ii) the implementation of machine learning algorithms to predict machine parameters. Data visualization and analysis is also proposed to support business decision-making. As a proof-of-concept, the proposed architecture was utilized in Chapter 3 to enable mental fatigue detection by employing embedded microcontrollers and sensors.

Mental fatigue is a problem that negatively affects the productivity of workers of all ages. Mental fatigue's main detection techniques include EEG signals and HRV features derived from ECG signals. The main contribution of this study was showing the feasibility of deriving HRV features from PPG signals in a technique which is a more convenient, simpler, yet effective way to detect mental fatigue in 11 participants. An ATMT installed on an off-the-shelf tablet was utilized to induce mental fatigue. Also, the NASA PVT application installed on a commercial smartphone was utilized to measure participants' reactions. PPG signals were recorded before and after the ATMT using a PPG sensor produced by DFRobot.

After performing a statistical analysis on HRV features extracted from PPG signals, only statistically significant features were retained. The results indicate that NNI_20, NNI_50, and Std_HR significantly decreased in the mental fatigue state due to prolonged activation of SNS. On the other hand, Median_NNI increased, which implied a slower HR at fatigue state, consistent with previously conducted ECG-based studies.

Regarding the performance of the tested machine learning classifiers, the highest accuracy obtained was LR, ANN, and SGD at 93.8%, followed by DT and SVM at 87.5%. A multiple stage feature selection process used p-value, Gini index, and Pearson coefficients to eliminate any irrelevant features. An automatic moving window that incorporated machine learning models was developed and tested on an additional participant. The results indicate different thresholds for the top performing models, LR and ANN, and a slight fluctuation for the least accurate models such as KNN. Also, the developed automatic moving window and machine learning classifiers were integrated into an OPC UA server (Raspberry Pi) forming a human digital twin unit that continuously monitored and detected mental fatigue. Finally, the constructed human

digital twin unit was connected to the overall smart factory through the developed client/gateway architecture as a proof-of-concept.

4.2. Future Work

Future work for the proposed client/gateway-based architecture includes connecting additional embedded and industrial devices within the same network. Connecting more devices implies more generated data that leads to the utilization of cloud computation and storage. Cloud services providers offer a handful of tools which can be used for data visualization, business analysis, statistical analysis, machine learning, simulations, and more. Those tools can be extremely beneficial in fields such as predictive maintenance, failure prediction, production planning, inventory management, etc. Furthermore, the deployment of the developed architecture in an actual production facility should be explored to assess the architecture's performance in real-life scenarios.

For the mental fatigue detection experiment, future work includes recruiting more participants to generalize the research outcomes. Also, investigating other, more convenient sensor attachment locations, such as the wrist and ear, is highly recommended to enhance users' level of comfort and sensor wearability for continuous monitoring. To achieve that, a custom-designed case should be manufactured along with various hardware and software filters to eliminate motion-induced noises. Regarding the developed automatic mental fatigue detection algorithm, a real-time version of the algorithm must be validated. Furthermore, fine-tuning the machine learning models should be explored to boost their performance even further and avoid over-fitting problems.

Currently, a mental fatigue detection technique was integrated and successfully connected to Ignition. However, to ensure scalability and achieve the full potential of the smart factory concept, a full implementation in a real-life facility will be carried out. The full implementation will include multiple workers' digital twin units that are capable of detecting mental fatigue, connected with machines' digital twin units within the shop floor through the proposed communication bridge.

References

[1] V. Gunes, S. Peter, T. Givargis, and F. Vahid, “A Survey on Concepts, Applications, and Challenges in Cyber-Physical Systems,” *KSII Transactions on Internet and Information Systems (TIIS)*, vol. 8, no. 12, pp. 4242–4268, 2014, doi: 10.3837/tiis.2014.12.001.

[2] R. (Raj) Rajkumar, I. Lee, L. Sha, and J. Stankovic, “Cyber-physical systems: the next computing revolution,” in *Proceedings of the 47th Design Automation Conference*, in DAC ’10. New York, NY, USA: Association for Computing Machinery, Jun. 2010, pp. 731–736. doi: 10.1145/1837274.1837461.

[3] K. Wang, Y. Wang, J. O. Strandhagen, and T. Yu, *Advanced Manufacturing and Automation V*. WIT Press, 2016.

[4] O. Vermesan and P. Friess, Eds., *Internet of Things Applications - From Research and Innovation to Market Deployment*. Taylor & Francis, 2014. doi: 10.1201/9781003338628.

[5] B. Dafflon, N. Moalla, and Y. Ouzrout, “The challenges, approaches, and used techniques of CPS for manufacturing in Industry 4.0: a literature review,” *Int J Adv Manuf Technol*, vol. 113, no. 7, pp. 2395–2412, Apr. 2021, doi: 10.1007/s00170-020-06572-4.

[6] E. Sisinni, A. Saifullah, S. Han, U. Jennehag, and M. Gidlund, “Industrial Internet of Things: Challenges, Opportunities, and Directions,” *IEEE Transactions on Industrial Informatics*, vol. 14, no. 11, pp. 4724–4734, Nov. 2018, doi: 10.1109/TII.2018.2852491.

[7] M. M. Mabkhot, A. M. Al-Ahmari, B. Salah, and H. Alkhalefah, “Requirements of the Smart Factory System: A Survey and Perspective,” *Machines*, vol. 6, no. 2, Art. no. 2, Jun. 2018, doi: 10.3390/machines6020023.

[8] E. Tantik and R. Anderl, “Integrated Data Model and Structure for the Asset Administration Shell in Industrie 4.0,” *Procedia CIRP*, vol. 60, pp. 86–91, Jan. 2017, doi: 10.1016/j.procir.2017.01.048.

[9] R. Söderberg, K. Wärmefjord, J. S. Carlson, and L. Lindkvist, “Toward a Digital Twin for real-time geometry assurance in individualized production,” *CIRP Annals*, vol. 66, no. 1, pp. 137–140, Jan. 2017, doi: 10.1016/j.cirp.2017.04.038.

[10] B. Chen, J. Wan, L. Shu, P. Li, M. Mukherjee, and B. Yin, “Smart Factory of Industry 4.0: Key Technologies, Application Case, and Challenges,” *IEEE Access*, vol. 6, pp. 6505–6519, 2018, doi: 10.1109/ACCESS.2017.2783682.

[11] P. Zawadzki and K. Żywicki, “Smart Product Design and Production Control for Effective Mass Customization in the Industry 4.0 Concept,” *Management and Production Engineering Review; 2016; No 3*, 2016, Accessed: Apr. 02, 2023. [Online]. Available: https://journals.pan.pl/dlibra/publication/121910/edition/106257

[12] P. Fantini, M. Pinzone, and M. Taisch, “Placing the operator at the centre of Industry 4.0 design: Modelling and assessing human activities within cyber-physical systems,” *Computers & Industrial Engineering*, vol. 139, p. 105058, Jan. 2020, doi: 10.1016/j.cie.2018.01.025.

[13] D. Romero, P. Bernus, O. Noran, J. Stahre, and Å. Fast-Berglund, “The Operator 4.0: Human Cyber-Physical Systems & Adaptive Automation Towards Human-Automation Symbiosis Work Systems,” in *Advances in Production Management Systems. Initiatives for a Sustainable World*, I. Nääs, O. Vendrametto, J. Mendes Reis, R. F. Gonçalves, M. T. Silva, G. von Cieminski, and D. Kiritsis, Eds., in IFIP Advances in Information and Communication Technology. Cham: Springer International Publishing, 2016, pp. 677–686. doi: 10.1007/978-3-319-51133-7_80.

[14] F. Ansari, S. Erol, and W. Sihn, “Rethinking Human-Machine Learning in Industry 4.0: How Does the Paradigm Shift Treat the Role of Human Learning?,” *Procedia Manufacturing*, vol. 23, pp. 117–122, Jan. 2018, doi: 10.1016/j.promfg.2018.04.003.

[15] M. Bandala, C. West, S. Monk, A. Montazeri, and C. J. Taylor, “Vision-Based Assisted Tele-Operation of a Dual-Arm Hydraulically Actuated Robot for Pipe Cutting and Grasping in Nuclear Environments,” *Robotics*, vol. 8, no. 2, Art. no. 2, Jun. 2019, doi: 10.3390/robotics8020042.

[16] J. Deng, G. Pang, Z. Zhang, Z. Pang, H. Yang, and G. Yang, “cGAN Based Facial Expression Recognition for Human-Robot Interaction,” *IEEE Access*, vol. 7, pp. 9848–9859, 2019, doi: 10.1109/ACCESS.2019.2891668.

[17] S. Sun, X. Zheng, B. Gong, J. García Paredes, and J. Ordieres-Meré, “Healthy Operator 4.0: A Human Cyber–Physical System Architecture for Smart Workplaces,” *Sensors*, vol. 20, no. 7, Art. no. 7, Jan. 2020, doi: 10.3390/s20072011.

[18] F. Longo, L. Nicoletti, and A. Padovano, “Smart operators in industry 4.0: A human-centered approach to enhance operators’ capabilities and competencies within the new smart factory context,” *Computers & Industrial Engineering*, vol. 113, pp. 144–159, Nov. 2017, doi: 10.1016/j.cie.2017.09.016.

[19] B. Salah, M. H. Abidi, S. H. Mian, M. Krid, H. Alkhalefah, and A. Abdo, “Virtual Reality-Based Engineering Education to Enhance Manufacturing Sustainability in Industry 4.0,” *Sustainability*, vol. 11, no. 5, Art. no. 5, Jan. 2019, doi: 10.3390/su11051477.

[20] L. Kassner, P. Hirmer, M. Wieland, F. Steimle, J. Königsberger, and B. Mitschang, “The Social Factory: Connecting People, Machines and Data in Manufacturing for Context-Aware Exception Escalation,” presented at the Hawaii International Conference on System Sciences, 2017. doi: 10.24251/HICSS.2017.202.

[21] F. Tao and M. Zhang, “Digital Twin Shop-Floor: A New Shop-Floor Paradigm Towards Smart Manufacturing,” *IEEE Access*, vol. 5, pp. 20418–20427, 2017, doi: 10.1109/ACCESS.2017.2756069.

[22] S. Shaikh and V. Chitre, “Healthcare monitoring system using IoT,” in *2017 International Conference on Trends in Electronics and Informatics (ICEI)*, May 2017, pp. 374–377. doi: 10.1109/ICOEI.2017.8300952.

[23] R. Kumar and M. P. Rajasekaran, “An IoT based patient monitoring system using raspberry Pi,” in *2016 International Conference on Computing Technologies and Intelligent Data Engineering (ICCTIDE’16)*, Jan. 2016, pp. 1–4. doi: 10.1109/ICCTIDE.2016.7725378.

[24] V. D. Pasquale, V. De Simone, M. Radano, and S. Miranda, “Wearable devices for health and safety in production systems: a literature review,” *IFAC-PapersOnLine*, vol. 55, no. 10, pp. 341–346, Jan. 2022, doi: 10.1016/j.ifacol.2022.09.410.

[25] A. Baghdadi, F. M. Megahed, E. T. Esfahani, and L. A. Cavuoto, “A machine learning approach to detect changes in gait parameters following a fatiguing occupational task,” *Ergonomics*, vol. 61, no. 8, pp. 1116–1129, Aug. 2018, doi: 10.1080/00140139.2018.1442936.

[26] A. Abdelsattar, E. J. Park, and A. Marzouk, “An OPC UA Client/Gateway-Based Digital Twin Architecture of a SCADA System with Embedded System Connections,” in *2022 IEEE/ASME International Conference on Advanced Intelligent Mechatronics (AIM)*, Jul. 2022, pp. 798–803. doi: 10.1109/AIM52237.2022.9863367.

[27] K. Židek, J. Piteľ, M. Adámek, P. Lazorík, and A. Hošovský, “Digital Twin of Experimental Smart Manufacturing Assembly System for Industry 4.0 Concept,” in *Sustainability*, (Basel, Switzerland): MDPI AG, May 2020, p. 3658.

[28] D. Upadhyay and S. Sampalli, “SCADA (Supervisory Control and Data Acquisition) systems: Vulnerability assessment and security recommendations,” *Computers & Security*, vol. 89, p. 101666, Feb. 2020, doi: 10.1016/j.cose.2019.101666.

[29] L. O. Aghenta and M. T. Iqbal, “Low-Cost, Open Source IoT-Based SCADA System Design Using Thinger.IO and ESP32 Thing,” *Electronics*, vol. 8, no. 8, Art. no. 8, Aug. 2019, doi: 10.3390/electronics8080822.

[30] Y. Li, J. Jiang, C. Lee, and S. H. Hong, “Practical Implementation of an OPC UA TSN Communication Architecture for a Manufacturing System,” *IEEE Access*, vol. 8, pp. 200100–200111, 2020, doi: 10.1109/ACCESS.2020.3035548.

[31] A. Künzel, A. Puchta, P. Gönnheimer, and J. Fleischer, “Modular and flexible Automation Middleware based on LabVIEW and OPC UA,” *IOP Conf. Ser.: Mater. Sci. Eng.*, vol. 1193, no. 1, p. 012109, Oct. 2021, doi: 10.1088/1757-899X/1193/1/012109.

[32] U.-S. Choi, K.-J. Kim, S.-S. Lee, K.-S. Kim, and J. Kim, “A Simple Fatigue Condition Detection Method by using Heart Rate Variability Analysis,” in *Advances in Parallel and Distributed Computing and Ubiquitous Services*, J. J. (Jong H. Park, G. Yi, Y.-S. Jeong, and H. Shen, Eds., in Lecture Notes in Electrical Engineering. Singapore: Springer, 2016, pp. 203–208. doi: 10.1007/978-981-10-0068-3_27.

[33] P. Tucker, S. Folkard, and I. Macdonald, “Rest breaks and accident risk,” *The Lancet*, vol. 361, no. 9358, p. 680, Feb. 2003, doi: 10.1016/S0140-6736(03)12566-4.

[34] T. Yamauchi *et al.*, “Overwork-related disorders in Japan: recent trends and development of a national policy to promote preventive measures,” *Industrial Health*, vol. 55, no. 3, pp. 293–302, 2017, doi: 10.2486/indhealth.2016-0198.

[35] M. K. Chen, “The epidemiology of self-perceived fatigue among adults,” *Prev Med*, vol. 15, no. 1, pp. 74–81, Jan. 1986, doi: 10.1016/0091-7435(86)90037-x.

[36] T. Pawlikowska, T. Chalder, S. R. Hirsch, P. Wallace, D. J. Wright, and S. C. Wessely, “Population based study of fatigue and psychological distress,” *BMJ*, vol. 308, no. 6931, pp. 763–766, Mar. 1994, doi: 10.1136/bmj.308.6931.763.

[37] M. A. S. Boksem and M. Tops, “Mental fatigue: Costs and benefits,” *Brain Research Reviews*, vol. 59, no. 1, pp. 125–139, Nov. 2008, doi: 10.1016/j.brainresrev.2008.07.001.

[38] “Fatigue and fatigability in neurologic illnesses | Neurology.” https://n.neurology.org/content/80/4/409 (accessed Aug. 11, 2022).

[39] S. Sarkar and C. Parnin, “Characterizing and Predicting Mental Fatigue during Programming Tasks,” in *2017 IEEE/ACM 2nd International Workshop on Emotion Awareness in Software Engineering (SEmotion)*, May 2017, pp. 32–37. doi: 10.1109/SEmotion.2017.2.

[40] E.-M. Backé, A. Seidler, U. Latza, K. Rossnagel, and B. Schumann, “The role of psychosocial stress at work for the development of cardiovascular diseases: a systematic review,” *Int Arch Occup Environ Health*, vol. 85, no. 1, pp. 67–79, Jan. 2012, doi: 10.1007/s00420-011-0643-6.

[41] M. M. Goedendorp, C. J. Tack, E. Steggink, L. Bloot, E. Bazelmans, and H. Knoop, “Chronic Fatigue in Type 1 Diabetes: Highly Prevalent but Not Explained by Hyperglycemia or Glucose Variability,” *Diabetes Care*, vol. 37, no. 1, pp. 73–80, Dec. 2013, doi: 10.2337/dc13-0515.

[42] J. E. Bower *et al.*, “Screening, assessment, and management of fatigue in adult survivors of cancer: An American Society of Clinical Oncology clinical practice guideline adaptation,” *Journal of Clinical Oncology*, vol. 32, no. 17, pp. 1840–1850, 2014, doi: 10.1200/JCO.2013.53.4495.

[43] S. Adam *et al.*, “Identifying classes of the pain, fatigue, and depression symptom cluster in long-term prostate cancer survivors—results from the multi-regional Prostate Cancer Survivorship Study in Switzerland (PROCAS),” *Support Care Cancer*, vol. 29, no. 11, pp. 6259–6269, Nov. 2021, doi: 10.1007/s00520-021-06132-w.

[44] Q. Liu *et al.*, “Research on Channel Selection and Multi-Feature Fusion of EEG Signals for Mental Fatigue Detection,” *Entropy*, vol. 23, no. 4, p. 457, Apr. 2021, doi: 10.3390/e23040457.

[45] S. Huang, J. Li, P. Zhang, and W. Zhang, “Detection of mental fatigue state with wearable ECG devices,” *International Journal of Medical Informatics*, vol. 119, pp. 39–46, Nov. 2018, doi: 10.1016/j.ijmedinf.2018.08.010.

[46] D. Jing, S. Zhang, and Z. Guo, “Fatigue driving detection method for low-voltage and hypoxia plateau area: A physiological characteristic analysis approach,” *International Journal of Transportation Science and Technology*, vol. 9, no. 2, pp. 148–158, Jun. 2020, doi: 10.1016/j.ijtst.2020.01.002.

[47] J. Hochhalter *et al.*, “Coupling Damage-Sensing Particles to the Digitial Twin Concept,” NF1676L-18764, Apr. 2014. Accessed: Aug. 22, 2022. [Online]. Available: https://ntrs.nasa.gov/citations/20140006408

[48] P. Leitão, V. Mařík, and P. Vrba, “Past, Present, and Future of Industrial Agent Applications,” *IEEE Transactions on Industrial Informatics*, vol. 9, no. 4, pp. 2360–2372, Nov. 2013, doi: 10.1109/TII.2012.2222034.

[49] A. Fernbach, W. Kastner, S. Mätzler, and M. Wollschlaeger, “An OPC UA information model for cross-domain vertical integration in automation systems,” in *Proceedings of the 2014 IEEE Emerging Technology and Factory Automation (ETFA)*, Sep. 2014, pp. 1–8. doi: 10.1109/ETFA.2014.7005215.

[50] H. Haskamp, F. Orth, J. Wermann, and A. W. Colombo, “Implementing an OPC UA interface for legacy PLC-based automation systems using the Azure cloud: An ICPS-architecture with a retrofitted RFID system,” in *2018 IEEE Industrial Cyber-Physical Systems (ICPS)*, May 2018, pp. 115–121. doi: 10.1109/ICPHYS.2018.8387646.

[51] P. F. S. Melo, E. P. Godoy, P. Ferrari, and E. Sisinni, “Open Source Control Device for Industry 4.0 Based on RAMI 4.0,” *Electronics*, vol. 10(7), no. 869, Jun. 2021.

[52] F. TAO and M. ZHANG, “Digital Twin Shop-Floor: A New Shop-Floor Paradigm Towards Smart Manufacturing”.

[53] R. Y. Zhong, Q. Y. Dai, T. Qu, G. J. Hu, and G. Q. Huang, “RFID-enabled real-time manufacturing execution system for mass-customization production,” *Robotics and Computer-Integrated Manufacturing*, vol. 29, no. 2, pp. 283–292, Apr. 2013, doi: 10.1016/j.rcim.2012.08.001.

[54] T. Mizuya, M. Okuda, and T. Nagao, “A case study of data acquisition from field devices using OPC UA and MQTT,” in *2017 56th Annual Conference of the Society of Instrument and Control Engineers of Japan (SICE)*, Sep. 2017, pp. 611–614. doi: 10.23919/SICE.2017.8105594.

[55] M. Schleipen, “OPC UA supporting the automated engineering of production monitoring and control systems,” in *2008 IEEE International Conference on Emerging Technologies and Factory Automation*, Sep. 2008, pp. 640–647. doi: 10.1109/ETFA.2008.4638464.

[56] G. Caiza, A. Nuñez, C. A. Garcia, and M. V. Garcia, “Human Machine Interfaces Based on Open Source Web-Platform and OPC UA,” *Procedia Manufacturing*, vol. 42, pp. 307–314, 2020, doi: 10.1016/j.promfg.2020.02.089.

[57] R. Ala-Laurinaho, J. Autiosalo, A. Nikander, J. Mattila, and K. Tammi, “Data Link for the Creation of Digital Twins,” *IEEE Access*, vol. 8, pp. 228675–228684, 2020, doi: 10.1109/ACCESS.2020.3045856.

[58] R. Langmann and M. Stiller, “The PLC as a Smart Service in Industry 4.0 Production Systems,” *Applied sciences*, vol. 9, no. 18, p. 3815, Sep. 2019.

[59] M. Teplan, “FUNDAMENTALS OF EEG MEASUREMENT,” *MEASUREMENT SCIENCE REVIEW*, vol. 2, 2002.

[60] S. H. Fairclough, L. Venables, and A. Tattersall, “The influence of task demand and learning on the psychophysiological response,” *International Journal of Psychophysiology*, vol. 56, no. 2, pp. 171–184, May 2005, doi: 10.1016/j.ijpsycho.2004.11.003.

[61] C. Berka *et al.*, “EEG Correlates of Task Engagement and Mental Workload in Vigilance, Learning, and Memory Tasks,” *Aviation, Space, and Environmental Medicine*, vol. 78, no. 5, pp. B231–B244, May 2007.

[62] J. L. Andreassi, *Psychophysiology: human behavior and physiological response / John L. Andreassi.*, Fifth edition. Erlbaum Associates, 2007. Accessed: Aug. 31, 2022. [Online]. Available: https://www.taylorfrancis.com/books/9780203880340

[63] A. Jain, B. Abbas, O. Farooq, and S. K. Garg, “Fatigue detection and estimation using auto-regression analysis in EEG,” in *2016 International Conference on Advances in Computing, Communications and Informatics (ICACCI)*, Sep. 2016, pp. 1092–1095. doi: 10.1109/ICACCI.2016.7732190.

[64] L. J. Trejo, K. Kubitz, R. Rosipal, R. L. Kochavi, and L. D. Montgomery, “EEG-Based Estimation and Classification of Mental Fatigue,” *Psychology*, vol. 6, no. 5, Art. no. 5, Apr. 2015, doi: 10.4236/psych.2015.65055.

[65] C. Jacobé de Naurois, C. Bourdin, C. Bougard, and J.-L. Vercher, “Adapting artificial neural networks to a specific driver enhances detection and prediction of drowsiness,” *Accident Analysis & Prevention*, vol. 121, pp. 118–128, Dec. 2018, doi: 10.1016/j.aap.2018.08.017.

[66] S. Sumathi and D. M. Y. Sanavullah, “Comparative Study of QRS Complex Detection in ECG Based on Discrete Wavelet Transform,” vol. 2, no. 5, 2009.

[67] L. Biel, O. Pettersson, L. Philipson, and P. Wide, “ECG analysis: a new approach in human identification,” *IEEE Transactions on Instrumentation and Measurement*, vol. 50, no. 3, pp. 808–812, Jun. 2001, doi: 10.1109/19.930458.

[68] D. Jaworski, “Detection of sleep and wake states based on the combined use of actigraphy and ballistocardiography,” Apr. 30, 2019. https://summit.sfu.ca/item/19976 (accessed Feb. 06, 2023).

[69] F. Shaffer and J. P. Ginsberg, “An Overview of Heart Rate Variability Metrics and Norms,” *Frontiers in Public Health*, vol. 5, 2017, Accessed: Aug. 31, 2022. [Online]. Available: https://www.frontiersin.org/articles/10.3389/fpubh.2017.00258

[70] H.-G. Kim, E.-J. Cheon, D.-S. Bai, Y. H. Lee, and B.-H. Koo, “Stress and Heart Rate Variability: A Meta-Analysis and Review of the Literature,” *Psychiatry Investig*, vol. 15, no. 3, pp. 235–245, Mar. 2018, doi: 10.30773/pi.2017.08.17.

[71] M. R. Esco and A. A. Flatt, “Ultra-Short-Term Heart Rate Variability Indexes at Rest and Post-Exercise in Athletes: Evaluating the Agreement with Accepted Recommendations,” *Journal of Sports Science & Medicine*, vol. 13, no. 3, pp. 535–541, Sep. 2014.

[72] J. He, K. Li, X. Liao, P. Zhang, and N. Jiang, “Real-Time Detection of Acute Cognitive Stress Using a Convolutional Neural Network From Electrocardiographic Signal,” *IEEE Access*, vol. 7, pp. 42710–42717, 2019, doi: 10.1109/ACCESS.2019.2907076.

[73] K. Tsunoda, A. Chiba, K. Yoshida, T. Watanabe, and O. Mizuno, “Predicting Changes in Cognitive Performance Using Heart Rate Variability,” *IEICE Trans. Inf. & Syst.*, vol. E100.D, no. 10, pp. 2411–2419, 2017, doi: 10.1587/transinf.2016OFP0002.

[74] E. Nemati, M. J. Deen, and T. Mondal, “A wireless wearable ECG sensor for long-term applications,” *IEEE Communications Magazine*, vol. 50, no. 1, pp. 36–43, Jan. 2012, doi: 10.1109/MCOM.2012.6122530.

[75] C. Park, P. H. Chou, Y. Bai, R. Matthews, and A. Hibbs, “An ultra-wearable, wireless, low power ECG monitoring system,” in *2006 IEEE Biomedical Circuits and Systems Conference*, Nov. 2006, pp. 241–244. doi: 10.1109/BIOCAS.2006.4600353.

[76] D. Castaneda, A. Esparza, M. Ghamari, C. Soltanpur, and H. Nazeran, “A review on wearable photoplethysmography sensors and their potential future applications in health care,” *Int J Biosens Bioelectron*, vol. 4, no. 4, pp. 195–202, 2018, doi: 10.15406/ijbsbe.2018.04.00125.

[77] N. Selvaraj, A. Jaryal, J. Santhosh, K. K. Deepak, and S. Anand, “Assessment of heart rate variability derived from finger-tip photoplethysmography as compared to electrocardiography,” *Journal of Medical Engineering & Technology*, vol. 32, no. 6, pp. 479–484, Jan. 2008, doi: 10.1080/03091900701781317.

[78] G. Lu, F. Yang, J. A. Taylor, and J. F. Stein, “A comparison of photoplethysmography and ECG recording to analyse heart rate variability in healthy subjects,” *Journal of Medical Engineering & Technology*, vol. 33, no. 8, pp. 634–641, Nov. 2009, doi: 10.3109/03091900903150998.

[79] S. Singh, M. Kozłowski, I. García-López, Z. Jiang, and E. Rodriguez-Villegas, “Proof of Concept of a Novel Neck-Situated Wearable PPG System for Continuous Physiological Monitoring,” *IEEE Transactions on Instrumentation and Measurement*, vol. 70, pp. 1–9, 2021, doi: 10.1109/TIM.2021.3083415.

[80] O. Binsch, T. Wabeke, and P. Valk, “Comparison of three different physiological wristband sensor systems and their applicability for resilience- and work load monitoring,” in *2016 IEEE 13th International Conference on Wearable and Implantable Body Sensor Networks (BSN)*, Jun. 2016, pp. 272–276. doi: 10.1109/BSN.2016.7516272.

[81] N. Sviridova and K. Sakai, “Human photoplethysmogram: new insight into chaotic characteristics,” *Chaos, Solitons & Fractals*, vol. 77, pp. 53–63, Aug. 2015, doi: 10.1016/j.chaos.2015.05.005.

[82] D. Biswas *et al.*, “CorNET: Deep Learning Framework for PPG-Based Heart Rate Estimation and Biometric Identification in Ambulant Environment,” *IEEE Transactions on Biomedical Circuits and Systems*, vol. 13, no. 2, pp. 282–291, Apr. 2019, doi: 10.1109/TBCAS.2019.2892297.

[83] L.-D. Liao *et al.*, “Design and Implementation of a Multifunction Wearable Device to Monitor Sleep Physiological Signals,” *Micromachines*, vol. 11, no. 7, Art. no. 7, Jul. 2020, doi: 10.3390/mi11070672.

[84] M. Wang, Z. Li, Q. Zhang, and G. Wang, “Removal of Motion Artifacts in Photoplethysmograph Sensors during Intensive Exercise for Accurate Heart Rate Calculation Based on Frequency Estimation and Notch Filtering,” *Sensors*, vol. 19, no. 15, Art. no. 15, Jan. 2019, doi: 10.3390/s19153312.

[85] F. Scardulla, L. D’Acquisto, R. Colombarini, S. Hu, S. Pasta, and D. Bellavia, “A Study on the Effect of Contact Pressure during Physical Activity on Photoplethysmographic Heart Rate Measurements,” *Sensors*, vol. 20, no. 18, Art. no. 18, Jan. 2020, doi: 10.3390/s20185052.

[86] Y. Sun, J. Lim, J. Meng, K. Kwok, N. Thakor, and A. Bezerianos, “Discriminative Analysis of Brain Functional Connectivity Patterns for Mental Fatigue Classification,” *Ann Biomed Eng*, vol. 42, no. 10, pp. 2084–2094, Oct. 2014, doi: 10.1007/s10439-014-1059-8.

[87] L. Arsintescu, K. H. Kato, P. F. Cravalho, N. H. Feick, L. S. Stone, and E. E. Flynn-Evans, “Validation of a touchscreen psychomotor vigilance task,” *Accident Analysis & Prevention*, vol. 126, pp. 173–176, May 2019, doi: 10.1016/j.aap.2017.11.041.

[88] K. Mizuno *et al.*, “Mental fatigue-induced decrease in levels of several plasma amino acids,” *J Neural Transm (Vienna)*, vol. 114, no. 5, pp. 555–561, 2007, doi: 10.1007/s00702-006-0608-1.

[89] K. Mizuno, M. Tanaka, K. Yamaguti, O. Kajimoto, H. Kuratsune, and Y. Watanabe, “Mental fatigue caused by prolonged cognitive load associated with sympathetic hyperactivity,” *Behav Brain Funct*, vol. 7, no. 1, p. 17, 2011, doi: 10.1186/1744-9081-7-17.

[90] M. Patel, S. K. L. Lal, D. Kavanagh, and P. Rossiter, “Applying neural network analysis on heart rate variability data to assess driver fatigue,” *Expert Systems with Applications*, vol. 38, no. 6, pp. 7235–7242, Jun. 2011, doi: 10.1016/j.eswa.2010.12.028.

[91] W. Liang, J. Yuan, D. Sun, and M. Lin, “Changes in Physiological Parameters Induced by Indoor Simulated Driving: Effect of Lower Body Exercise at Mid-Term Break,” *Sensors*, vol. 9, no. 9, pp. 6913–6933, Sep. 2009, doi: 10.3390/s90906913.

[92] T. Chalder *et al.*, “Development of a fatigue scale,” *Journal of Psychosomatic Research*, vol. 37, no. 2, pp. 147–153, Feb. 1993, doi: 10.1016/0022-3999(93)90081-P.

[93] R. Champseix, L. Ribiere, and C. L. Couedic, “A Python Package for Heart Rate Variability Analysis and Signal Preprocessing,” *Journal of Open Research Software*, vol. 9, no. 1, Art. no. 1, Oct. 2021, doi: 10.5334/jors.305.

[94] H. Al-Libawy, A. Al-Ataby, W. Al-Nuaimy, and M. A. Al-Taee, “HRV-based operator fatigue analysis and classification using wearable sensors,” in *2016 13th International Multi-Conference on Systems, Signals & Devices (SSD)*, Mar. 2016, pp. 268–273. doi: 10.1109/SSD.2016.7473750.

[95] D. Zhang, X. Shen, and X. Qi, “Resting heart rate and all-cause and cardiovascular mortality in the general population: a meta-analysis,” *CMAJ*, vol. 188, no. 3, pp. E53–E63, Feb. 2016, doi: 10.1503/cmaj.150535.

[96] J. McNames and M. Aboy, “Reliability and accuracy of heart rate variability metrics versus ECG segment duration,” *Med Bio Eng Comput*, vol. 44, no. 9, pp. 747–756, Sep. 2006, doi: 10.1007/s11517-006-0097-2.

[97] T. Pham, Z. J. Lau, S. H. A. Chen, and D. Makowski, “Heart Rate Variability in Psychology: A Review of HRV Indices and an Analysis Tutorial,” *Sensors*, vol. 21, no. 12, Art. no. 12, Jan. 2021, doi: 10.3390/s21123998.

[98] N. Bouzida, A. Bendada, and X. P. Maldague, “Visualization of body thermoregulation by infrared imaging,” *Journal of Thermal Biology*, vol. 34, no. 3, pp. 120–126, Apr. 2009, doi: 10.1016/j.jtherbio.2008.11.008.

[99] R. L. Burr, “Interpretation of Normalized Spectral Heart Rate Variability Indices In Sleep Research: A Critical Review,” *Sleep*, vol. 30, no. 7, pp. 913–919, Jul. 2007.

[100] H. Han, X. Guo, and H. Yu, “Variable selection using Mean Decrease Accuracy and Mean Decrease Gini based on Random Forest,” in *2016 7th IEEE International Conference on Software Engineering and Service Science (ICSESS)*, Aug. 2016, pp. 219–224. doi: 10.1109/ICSESS.2016.7883053.

[101] Y. Yue, D. Liu, S. Fu, and X. Zhou, “Heart Rate and Heart Rate Variability as Classification Features for Mental Fatigue Using Short-Term PPG Signals Via Smartphones Instead of ECG Recordings,” in *2021 13th International Conference on Communication Software and Networks (ICCSN)*, Jun. 2021, pp. 370–376. doi: 10.1109/ICCSN52437.2021.9463614.

[102] P. Qi *et al.*, “Neural Mechanisms of Mental Fatigue Revisited: New Insights from the Brain Connectome,” *Engineering*, vol. 5, no. 2, pp. 276–286, Apr. 2019, doi: 10.1016/j.eng.2018.11.025.

[103] D. Gui *et al.*, “Resting spontaneous activity in the default mode network predicts performance decline during prolonged attention workload,” *NeuroImage*, vol. 120, pp. 323–330, Oct. 2015, doi: 10.1016/j.neuroimage.2015.07.030.

[104] Y. Sun, J. Lim, K. Kwok, and A. Bezerianos, “Functional cortical connectivity analysis of mental fatigue unmasks hemispheric asymmetry and changes in small-world networks,” *Brain and Cognition*, vol. 85, pp. 220–230, Mar. 2014, doi: 10.1016/j.bandc.2013.12.011.

[105] G. N. Dimitrakopoulos *et al.*, “Functional Connectivity Analysis of Mental Fatigue Reveals Different Network Topological Alterations Between Driving and Vigilance Tasks,” *IEEE Transactions on Neural Systems and Rehabilitation Engineering*, vol. 26, no. 4, pp. 740–749, Apr. 2018, doi: 10.1109/TNSRE.2018.2791936.

[106] Y. Ma, F. Tian, Q. Zhao, and B. Hu, “Design and Application of Mental Fatigue Detection System Using Non-Contact ECG and BCG Measurement,” in *2018 IEEE International Conference on Bioinformatics and Biomedicine (BIBM)*, Dec. 2018, pp. 1508–1513. doi: 10.1109/BIBM.2018.8621578.

[107] D. Fang, Z. Jiang, M. Zhang, and H. Wang, “An experimental method to study the effect of fatigue on construction workers’ safety performance,” *Safety Science*, vol. 73, pp. 80–91, Mar. 2015, doi: 10.1016/j.ssci.2014.11.019.

[108] J. Bowen, A. Hinze, and C. Griffiths, “Investigating real-time monitoring of fatigue indicators of New Zealand forestry workers,” *Accident Analysis & Prevention*, vol. 126, pp. 122–141, May 2019, doi: 10.1016/j.aap.2017.12.010.

Appendix A.

Ethics Approval

SFU RESEARCH ETHICS

Minimal Risk Approval – Delegated

Study Number: 30001033
Study Title: Development of a mental fatigue detection algorithm using Photoplethysmography (PPG) sensor

Approval Date: September 21, 2022
Principal Investigator: Edward Park
Faculty/Department: Applied Sciences

Expiration Date: September 21, 2023
SFU Position: Faculty

Student Lead: Ahmad Abdelsattar
SFU Collaborator(s): Amr Marzouk
Research Personnel: N/A
External Collaborator(s): N/A

Funder: NSERC
Funding Title: Sensor Fusion for Health-tracking Wearable Devices and Internet of Things
Funding Number: R611557

Document(s) Approved in this Application:
Consent Form, version 1 dated September 21, 2022
Recruitment Email, version 1 dated September 20, 2022
Fatigue Self-reported Scale, version dated September 14, 2022
NASA PVT Test Description Document, version 1 dated Septembe3r 17, 2022

Document(s) Acknowledged in this Application:
Supervisory Committee Ethics Draft Approval, dated September 2, 2022
Study Description Document

Research Team Members TCPS 2 CORE Training Certificates:
Ahmad Abdelsattar, dated August 22, 2022

The application for ethical review and the document(s) listed above have been reviewed and the procedures were found to be acceptable on ethical grounds for research involving human participants.

The approval for this Study expires on the **Expiration Date. An Annual Renewal must be completed every year prior to the Expiration Date. Failure to submit an Annual Renewal will lead to your study being suspended and potentially terminated.** The Board reviews and may amend decisions or subsequent amendments made independently by the authorized delegated reviewer at its regular monthly meeting.

This letter is your official ethics approval documentation for this project. Please keep this document for reference purposes.

This study has been approved by an authorized delegated reviewer.

SIMON FRASER UNIVERSITY ENGAGING THE WORLD Page **1** of **1**

Appendix B.

Consent Form

SFU SIMON FRASER UNIVERSITY

Consent Form

Development of a mental fatigue detection algorithm using Photoplethysmography (PPG) sensor.

Principal Investigator: Dr. Edward Park, Professor at School of Mechatronic Systems Engineering, Simon Fraser University. Dr. Amr Marzouk, Senior Lecturer at School of Mechatronic Systems Engineering, Simon Fraser University. Student Lead: Ahmad Abdelsattar, MASc candidate at School of Mechatronic Systems Engineering, Simon Fraser University.

This study is part of Ahmad Abdelsattar's MASc graduate degree and will be published in a journal paper as part of his MASc thesis.

Participant ID:

Age:

Gender:

Sponsor

This study is funded by NSERC Discovery Grant entitled "Sensor Fusion for Health-tracking Wearable Devices and Internet of Things".

Study Purpose

We are doing this study to learn more about mental fatigue pattern for healthy adults over the age of 19. We want to learn more about mental fatigue patterns and how to properly measure and represent it without interrupting their normal daily work. This study aims to investigate the mental fatigue patters based on physiological data, so breaks can be more effective. If you have any concerns about mental fatigue patterns before or after the experiment, please seek the advice of a medical doctor or a specialist for more information.

Voluntary Participation

Your participation is voluntary and will occur before and after performing tasks that require mental operations. You may choose to withdraw at anytime during the study if you consider the experiment inconvenient.

SFU SIMON FRASER UNIVERSITY

Study Instrumentation

This section is to introduce the equipment that will be used in the experiment. If you have any question, please don't hesitate to ask the Student Lead.

a) DFRobot Pulse Sensor Heart Rate Sensor heartbeat Pulse Sensor. The sensor will detect the PPG signal from the participant's finger. The operating input voltage ranges between 3-5 volts. The PPG data will be in the analog form and range between 0-5 volts.

b) Psychomotor Vigilance Test (PVT) device will be provided to the user to perform the test. The NASA PVT application is installed on a tablet (please refer to appendix B). The simple test will be used within the application to measure the reaction time. The reaction time will be measured by pressing on the tablet's touch screen. The user will have the opportunity to orient and configure the dominant hand in the application to maximize comfort before starting the test such as holding it in their right or left hand, placing on the desk or lap and clicking whichever button is most convenient. The application only stores stopwatch times (in milliseconds) and will be exported by the research team into the database for additional storage. No personal information is recorded on the PVT application itself. The participant will be requested to monitor the initialization, collection, and data exporting process to ensure the highest level of confidentiality.

Study Procedure

If you choose to participate in this study, the study will proceed like this:

- A self-report fatigue questionnaire will be provided to you on physical paper to gather basic physiological information regarding your level of fatigue.
- You will be briefed on the sensors and devices before the study begins.
- A PPG sensor will be attached to your preferred finger and data will be recorded for 10 minutes.
- A 5-minute bio break will be given.
- A tablet with a PVT application will be given to you to measure the reaction time.
- You will be guided through the PVT settings to choose the most convenient settings, and the PVT will last for 5 minutes.
- A tablet with a trail making application will be given to you, and a timer will be set to 1 hour.

- The tablet will be collected after 1 hour.
- A second self-report fatigue questionnaire will be provided to you on a physical paper to gather physiological information after performing the tests.
- A PPG sensor will be attached to your preferred finger and data will be recorded for 10 minutes.
- The tablet with PVT application installed will be given to you to measure you reaction time, and it will last for 5 minutes.

The expected total duration of the experiment is approximately 2 hours.

Potential Risks of the Study

- The risk is no more than playing a video game on a tablet for 1 hour

Opting Out of The Study

- You may opt out the experiment anytime before the test day by sending an email or a text message to the Student Lead
- You may opt out during the experiment at anytime without reasons, and the collected data will be deleted immediately

Benefits of the Study

- Gathering data on how people mental fatigue states will be beneficial for developing algorithms and devices that detect mental fatigue patterns of people.

- One of the benefits is to be able to detect when someone is mentally fatigued or alert without disrupting their daily tasks. This will result in a more efficient way to determine break times and to prevent any risks associated with working while being fatigued.

Confidentiality

This study is part of a graduate study and therefore the results from the experiments will be used in a graduate thesis and a journal paper. Each participant will be presented in the thesis by generally referring to them by participant ID without using any personal names. Your physiological data such as name, height and weight etc. will not be collected as they do not influence the results.

SFU SIMON FRASER UNIVERSITY

The data and academic papers directly referencing this data may be referenced in other articles written in the future. Only the Student Lead and the PI will have access to participant personal information and both the PI and the Student Lead will have access to the data collected from the study.

After the study results have been completed, the PI will store all related data on his local hard drive for approximately 2 years. Future use of the collected data includes performing advanced statistical analysis such as: t-test, F-test, p-value, Pearson and Spearman correlation coefficients.

Organizational Permission

Permission to conduct this research study from the Simon Fraser University Ethics Board.

Study Results

The study results will be published in a graduate thesis and may also be published in academic journals and articles. You may request to go over your results after the study is concluded with the PI and the Student Lead. However, the results will not be available right away after the study and you may schedule a time to see your results.

Contact Information for Questions about the Study

If you have any questions about your rights as a research participant or concerns about the way you were treated in this study, please don't hesitate to reach out the research team using the following contacts:

Student Lead: Ahmad Abdelsattar
Email:
Phone: [redacted]

Principal Investigator: Edward Park
Email:
Phone: [redacted]

SFU SIMON FRASER UNIVERSITY

Contact for Concerns or Complaints

If you have any concerns about your rights as a research participant and/or your experiences while participating in this study, please contact the Director, SFU Office of Research Ethics, at dore@sfu.ca or 778-782-6593.

Participant Consent

Taking part in this study is entirely up to you. You have the right to refuse to participate in this study. If you decide to take part, you may choose to pull out of the study at any time without giving a reason and without any negative impact. The records of this consent form will be kept for 2 years. The data will be retained with the PI for the whole mentioned duration and will be safely destroyed after.

Participant Signature: Date:

Appendix C.

Significant Features Box Plots

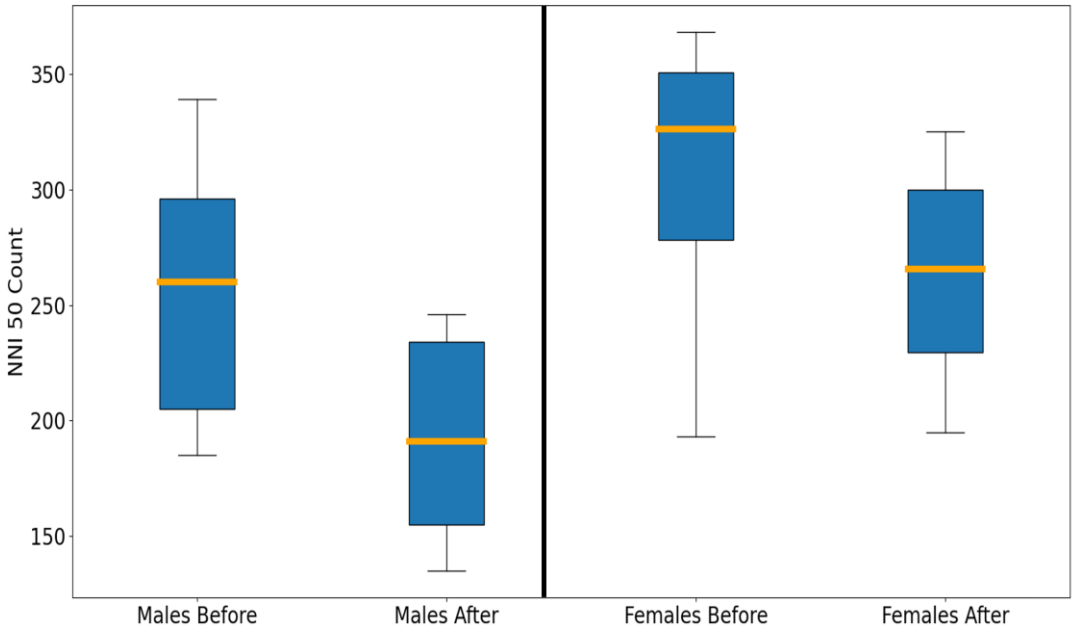

Figure C.1. NNI 50 count for both genders (left males and right females) before and after the ATMT

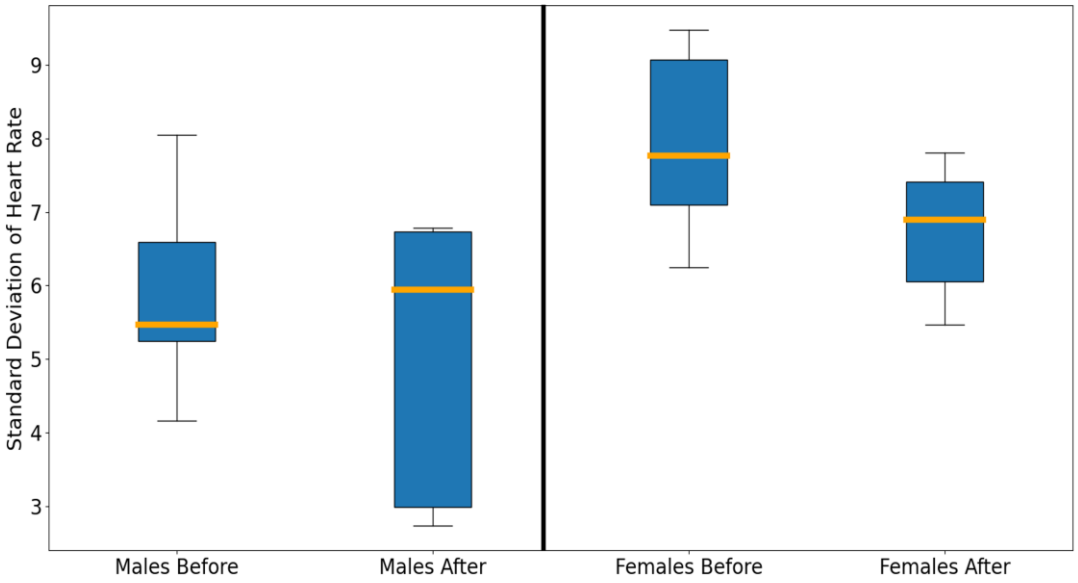

Figure C.2. Standard deviation of heart rate for both genders (left males and right females) before and after the ATMT

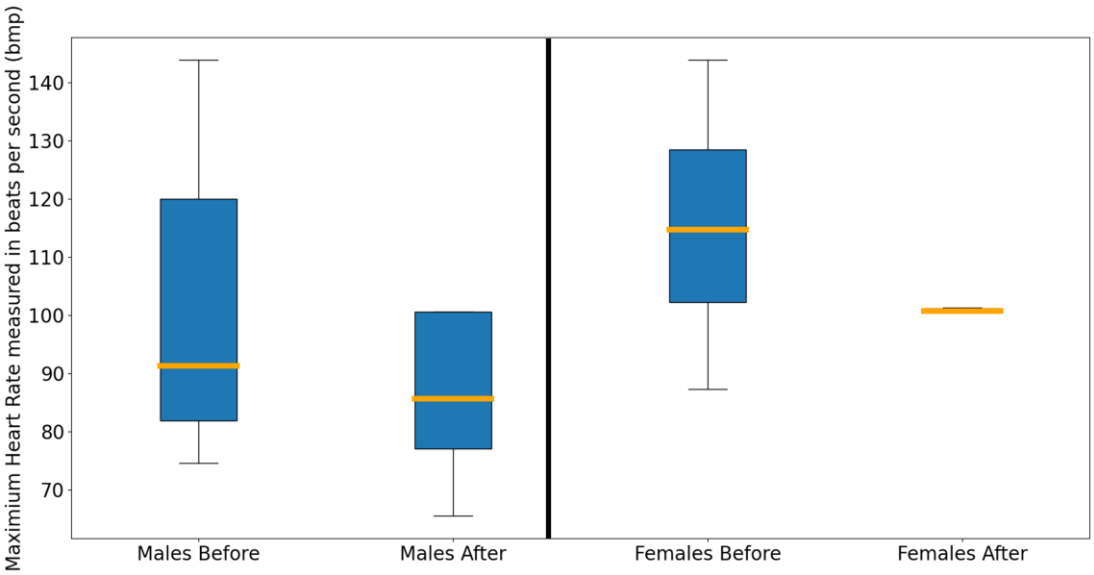

Figure C.3. Maximum heart rate in (bpm) for both genders (left males and right females) before and after the ATMT

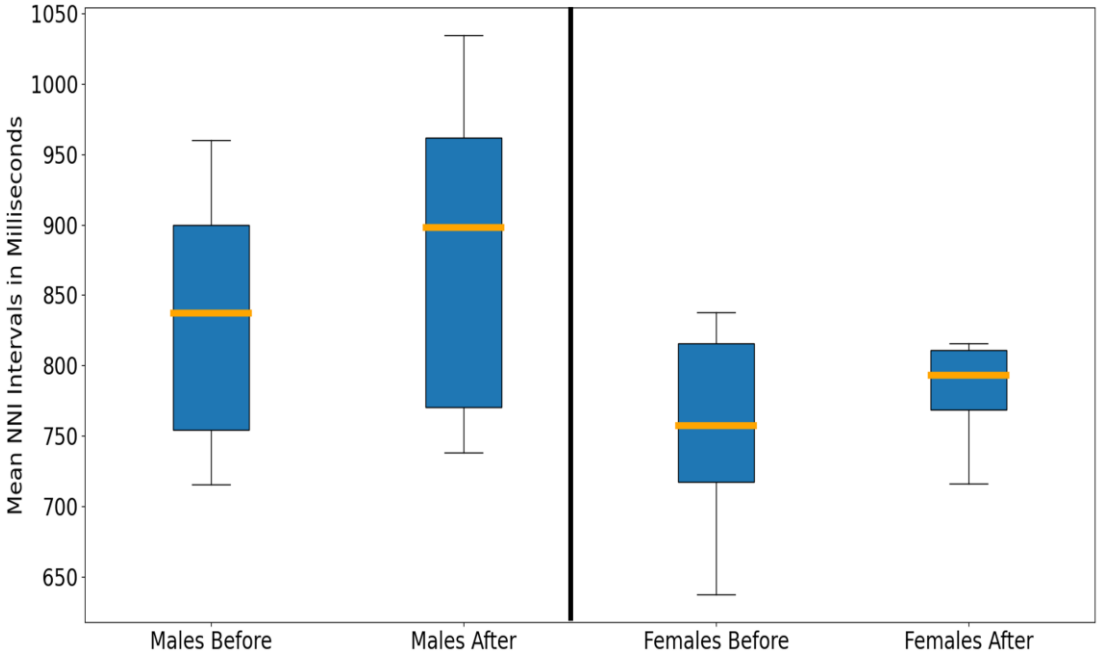

Figure C.4. Mean NNI in milliseconds for both genders (left males and right females) before and after the ATMT

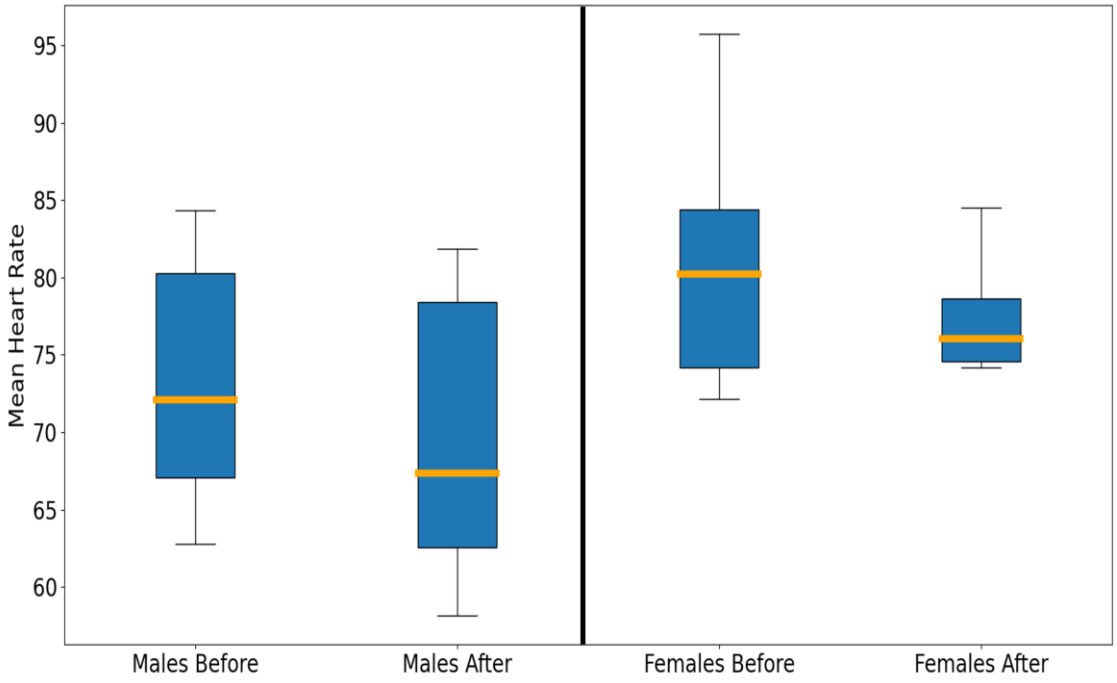

Figure C.5. Mean heart rate for both genders (left females and right males) before and after the ATMT

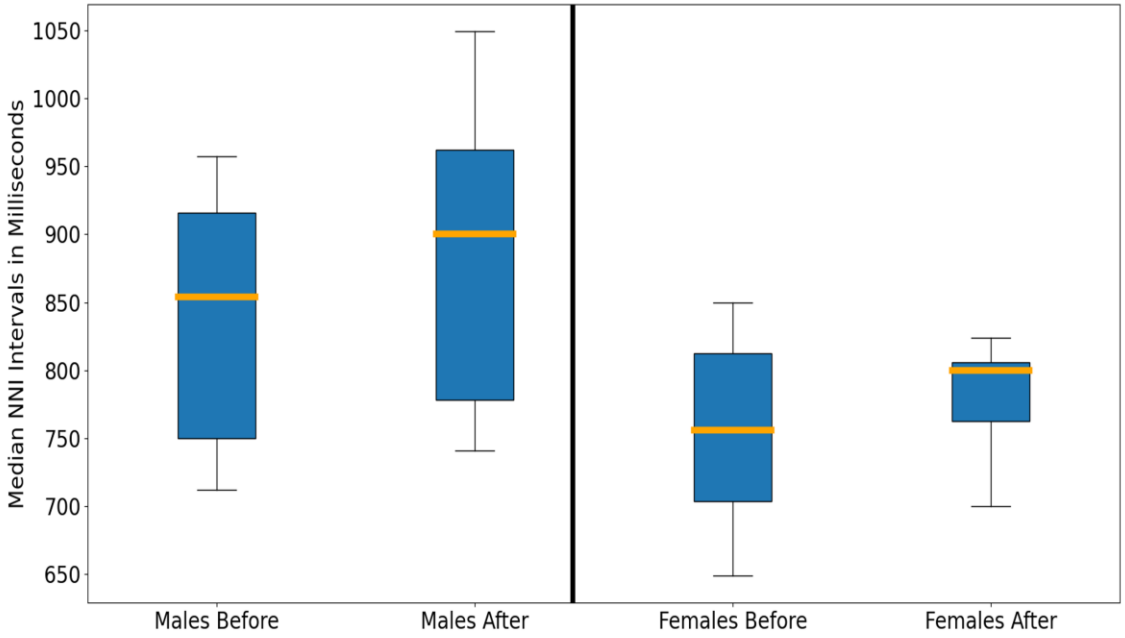

Figure C.6. Median NNI in milliseconds for both genders (left males and right femalesss) before and after the ATMT

Appendix D.

ANOVA Scores

Analysis of Variance Results

F-statistic value = 8.83244

P-value = 0.01565

Data Summary				
Groups	N	Mean	Std. Dev.	Std. Error
Group 1	6	552.6667	60.9284	24.8739
Group 2	5	467.4	20.2682	9.0642

ANOVA Summary					
Source	Degrees of Freedom DF	Sum of Squares SS	Mean Square MS	F-Stat	P-Value
Between Groups	1	19828.3913	19828.3913	8.8324	0.0157
Within Groups	9	20204.5494	2244.9499		
Total:	10	40032.9406			

Figure D.1. NNI 20 count at rest for both genders. Group 1 represents females and group represents males

Analysis of Variance Results

F-statistic value = 12.12711

P-value = 0.00691

Data Summary				
Groups	N	Mean	Std. Dev.	Std. Error
Group 1	6	506	44.7169	18.2556
Group 2	5	418.2	37.4326	16.7404

ANOVA Summary					
Source	Degrees of Freedom DF	Sum of Squares SS	Mean Square MS	F-Stat	P-Value
Between Groups	1	21024.1091	21024.1091	12.1271	0.0069
Within Groups	9	15602.8039	1733.6449		
Total:	10	36626.913			

Figure D.2. NNI 20 count at fatigue for both genders. Group 1 represents females and group 2 represents males

Analysis of Variance Results

F-statistic value = 1.52523

P-value = 0.2481

Data Summary				
Groups	N	Mean	Std. Dev.	Std. Error
Group 1	6	305.6667	66.2923	27.0637
Group 2	5	257	63.5256	28.4095

ANOVA Summary					
Source	Degrees of Freedom DF	Sum of Squares SS	Mean Square MS	F-Stat	P-Value
Between Groups	1	6459.4028	6459.4028	1.5252	0.2481
Within Groups	9	38115.3526	4235.0392		
Total:	10	44574.7554			

Figure D.3. NNI 50 count at rest for both genders. Group 1 represents females and group 2 represents males

Analysis of Variance Results

F-statistic value = 5.53665

P-value = 0.04309

Data Summary				
Groups	N	Mean	Std. Dev.	Std. Error
Group 1	6	263.3333	51.251	20.9231
Group 2	5	192.2	48.2151	21.5625

ANOVA Summary					
Source	Degrees of Freedom DF	Sum of Squares SS	Mean Square MS	F-Stat	P-Value
Between Groups	1	13799.8537	13799.8537	5.5366	0.0431
Within Groups	9	22432.1085	2492.4565		
Total:	10	36231.9622			

Figure D.4. NNI 50 count at fatigue for both genders. Group 1 represents females and group 2 represents males

Analysis of Variance Results

F-statistic value = 4.65897

P-value = 0.05922

Data Summary				
Groups	N	Mean	Std. Dev.	Std. Error
Group 1	6	8.4259	2.2295	0.9102
Group 2	5	5.9019	1.4756	0.6599

ANOVA Summary					
Source	Degrees of Freedom DF	Sum of Squares SS	Mean Square MS	F-Stat	P-Value
Between Groups	1	17.3743	17.3743	4.659	0.0592
Within Groups	9	33.5629	3.7292		
Total:	10	50.9372			

Figure D.5. Standard deviation of heart rate at rest state for both genders. Group 1 represents females and group 2 is males

Analysis of Variance Results

F-statistic value = 3.45816

P-value = 0.09587

Data Summary				
Groups	N	Mean	Std. Dev.	Std. Error
Group 1	6	6.7365	0.9304	0.3798
Group 2	5	5.0351	2.0136	0.9005

ANOVA Summary					
Source	Degrees of Freedom DF	Sum of Squares SS	Mean Square MS	F-Stat	P-Value
Between Groups	1	7.8948	7.8948	3.4582	0.0959
Within Groups	9	20.5466	2.283		
Total:	10	28.4414			

Figure D.6. Standard deviation of heart rate at fatigue for both genders. Group 1 is females and group 2 is males.

Analysis of Variance Results

F-statistic value = 4.39322

P-value = 0.06554

Data Summary				
Groups	N	Mean	Std. Dev.	Std. Error
Group 1	6	754.8333	78.6064	32.0909
Group 2	5	886	127.7008	57.1095

ANOVA Summary					
Source	Degrees of Freedom DF	Sum of Squares SS	Mean Square MS	F-Stat	P-Value
Between Groups	1	46921.9178	46921.9178	4.3932	0.0655
Within Groups	9	96124.8079	10680.5342		
Total:	10	143046.7257			

Figure D.7. Median NNI at rest state for both genders. Group 1 represents females and group 2 represents males.

Analysis of Variance Results

F-statistic value = 3.60373

P-value = 0.09013

Data Summary				
Groups	N	Mean	Std. Dev.	Std. Error
Group 1	6	780.3333	46.5174	18.9906
Group 2	5	886	127.7008	57.1095

ANOVA Summary					
Source	Degrees of Freedom DF	Sum of Squares SS	Mean Square MS	F-Stat	P-Value
Between Groups	1	30451.2313	30451.2313	3.6037	0.0901
Within Groups	9	76049.3198	8449.9244		
Total:	10	106500.5511			

Figure D.8. Median NNI at fatigue for both genders. Group 1 represents females and group 2 represents males.

Analysis of Variance Results

F-statistic value = 2.15476

P-value = 0.17619

Data Summary				
Groups	N	Mean	Std. Dev.	Std. Error
Group 1	6	754.8864	76.9277	31.4056
Group 2	5	833.3629	100.7031	45.0358

ANOVA Summary					
Source	Degrees of Freedom DF	Sum of Squares SS	Mean Square MS	F-Stat	P-Value
Between Groups	1	16796.0756	16796.0756	2.1548	0.1762
Within Groups	9	70153.8125	7794.8681		
Total:	10	86949.8881			

Figure D.9. Mean NNI at rest for both genders. Group 1 represents females and group 2 represents males.

Analysis of Variance Results

F-statistic value = 3.3535

P-value = 0.1003

Data Summary				
Groups	N	Mean	Std. Dev.	Std. Error
Group 1	6	782.5696	38.1458	15.573
Group 2	5	880.5017	125.4215	56.0902

ANOVA Summary					
Source	Degrees of Freedom DF	Sum of Squares SS	Mean Square MS	F-Stat	P-Value
Between Groups	1	26156.4442	26156.4442	3.3535	0.1003
Within Groups	9	70197.7209	7799.7468		
Total:	10	96354.1651			

Figure D.10. Mean NNI at fatigue for both genders. Group 1 represents females and group 2 represents males

Analysis of Variance Results

F-statistic value = 2.04196

P-value = 0.18679

Data Summary				
Groups	N	Mean	Std. Dev.	Std. Error
Group 1	6	81.0509	8.9153	3.6396
Group 2	5	73.3135	8.9753	4.0139

ANOVA Summary					
Source	Degrees of Freedom DF	Sum of Squares SS	Mean Square MS	F-Stat	P-Value
Between Groups	1	163.2746	163.2746	2.042	0.1868
Within Groups	9	719.6369	79.9597		
Total:	10	882.9115			

Figure D.11. Mean heart rate at rest for both genders. Group 1 represents females and group 2 represents males

Analysis of Variance Results

F-statistic value = 2.98989

P-value = 0.11785

Data Summary				
Groups	N	Mean	Std. Dev.	Std. Error
Group 1	6	77.3987	3.963	1.6179
Group 2	5	69.6505	10.1775	4.5515

ANOVA Summary					
Source	Degrees of Freedom DF	Sum of Squares SS	Mean Square MS	F-Stat	P-Value
Between Groups	1	163.7307	163.7307	2.9899	0.1178
Within Groups	9	492.8529	54.7614		
Total:	10	656.5836			

Figure D.12. Mean heart rate at fatigue for both genders. Group 1 represents females and group 2 represents males

Analysis of Variance Results

F-statistic value = 0.75301

P-value = 0.40807

Data Summary				
Groups	N	Mean	Std. Dev.	Std. Error
Group 1	6	115.3404	20.7335	8.4644
Group 2	5	102.3606	28.9062	12.9272

ANOVA Summary					
Source	Degrees of Freedom DF	Sum of Squares SS	Mean Square MS	F-Stat	P-Value
Between Groups	1	459.4778	459.4778	0.753	0.4081
Within Groups	9	5491.6637	610.1849		
Total:	10	5951.1415			

Figure D.13. Maximum heart rate at rest for both genders. Group 1 represents females and group 2 represents males

Analysis of Variance Results

F-statistic value = 0.43328

P-value = 0.52686

Data Summary				
Groups	N	Mean	Std. Dev.	Std. Error
Group 1	6	104.089	10.4318	4.2588
Group 2	5	95.1559	31.5303	14.1008

ANOVA Summary					
Source	Degrees of Freedom DF	Sum of Squares SS	Mean Square MS	F-Stat	P-Value
Between Groups	1	217.6371	217.6371	0.4333	0.5269
Within Groups	9	4520.7515	502.3057		
Total:	10	4738.3886			

Figure D.14. Maximum heart rate at fatigue for both genders. Group 1 represents females and group 2 represents males

Appendix E.

HRV Features for All Participants

Table E.1. Complete selected HRV features for all participants at both states

Data Index	NNI_20	NNI_50	Std_HR	Mean_NNI	Mean HR	Median_NNI	Max_HR
Participant 1 After	476	234	5.81	785.35	76.81	800	101.35
Participant 2 After	461	195	6.99	763.11	79.21	750	100.67
Participant 3 After	518	301	7.54	814.59	74.36	824	100.84
Participant 4 After	384	191	6.77	770.58	78.43	778	100.67
Participant 5 After	453	234	6.72	738.04	81.83	741	146.69
Participant 6 After	588	325	7.80	715.92	84.52	700	125
Participant 7 After	390	155	2.73	1034.25	58.14	1049	65.57
Participant 8 After	400	135	2.98	961.76	62.52	962	77.12
Participant 9 After	500	228	5.47	800.89	75.30	800	96
Participant 10 After	464	246	5.94	897.86	67.32	900	85.71
Participant 11 After	493	297	6.78	815.52	74.16	808	100.67
Participant 1 Before	521	263	7.87	795.11	76.11	800	143.88

Data Index	NNI_20	NNI_50	Std_HR	Mean_NNI	Mean HR	Median_NNI	Max_HR
Participant 2 Before	511	193	7.65	716.43	84.41	701	109.28
Participant 3 Before	551	328	9.47	719.91	84.34	712	120.24
Participant 4 Before	463	205	8.04	754.58	80.28	750	120
Participant 5 Before	472	339	6.58	715.34	84.36	712	143.88
Participant 6 Before	674	358	12.40	637.39	95.72	649	131.29
Participant 7 Before	450	260	4.16	959.80	62.78	957.5	74.62
Participant 8 Before	500	185	5.24	899.89	67.06	916	81.96
Participant 9 Before	526	324	6.24	837.75	72.14	850	87.33
Participant 10 Before	452	296	5.46	837.18	72.06	854	91.32
Participant 11 Before	533	368	6.90	822.69	73.55	817	100